ORIGINAL ARTICLE

Densities and Laminar Distributions of Kv3.1b-, PV-, GABA-, and SMI-32-Immunoreactive Neurons in Macaque Area V1

Jenna G. Kelly[1], Virginia García-Marín[1], Bernardo Rudy[2]
and Michael J. Hawken[1]

[1]Center for Neural Science, New York University, New York, NY 10003, USA and [2]New York University Neuroscience Institute, New York University School of Medicine, Smilow Research Building Sixth Floor, 522 First Ave., New York, NY 10016, USA

Address correspondence to Michael Hawken, Center for Neural Science, New York University, 4 Washington Place, New York, NY 10003, USA.
E-mail: mjh2@nyu.edu

Abstract

The Kv3.1b potassium channel subunit is associated with narrow spike widths and fast-spiking properties. In macaque primary visual cortex (V1), subsets of neurons have previously been found to be Kv3.1b-immunoreactive (ir) but not parvalbumin (PV)-ir or not GABA-ir, suggesting that they may be both fast-spiking and excitatory. This population includes Meynert cells, the large layer 5/6 pyramidal neurons that are also labeled by the neurofilament antibody SMI-32. In the present study, triple immunofluorescence labeling and confocal microscopy were used to measure the distribution of Kv3.1b-ir, non-PV-ir, non-GABA-ir neurons across cortical depth in V1, and to determine whether, like the Meynert cells, other Kv3.1b-ir excitatory neurons were also SMI-32-ir pyramidal neurons. We found that Kv3.1b-ir, non-PV-ir, non-GABA-ir neurons were most prevalent in the M pathway-associated layers 4 Cα and 4B. GABAergic neurons accounted for a smaller fraction (11%) of the total neuronal population across layers 1–6 than has previously been reported. Of Kv3.1b-ir neurons, PV expression reliably indicated GABA expression. Kv3.1b-ir, non-PV-ir neurons varied in SMI-32 coimmunoreactivity. The results suggest the existence of a heterogeneous population of excitatory neurons in macaque V1 with the potential for sustained high firing rates, and these neurons were particularly abundant in layers 4B and 4 Cα.

Key words: excitatory neurons, fast-spiking, Kv3.1b potassium channel subunit, parvalbumin, primary visual cortex

Introduction

The dynamics of the Kv3.1b potassium channel subunit enable expression of the fast-spiking phenotype—typically associated with parvalbumin (PV) expressing interneurons (Kawaguchi and Kubota 1993, 1998; Cauli et al. 1997; Zaitsev et al. 2005; Povysheva et al. 2008; Tremblay et al. 2016)—by narrowing spike width, shortening the refractory period that limits inter-spike interval, minimizing sodium channel inactivation, and ensuring complete membrane repolarization with a resurgent potassium current (Du et al. 1996; Wang et al. 1998; Erisir et al. 1999; Rudy and McBain 2001; Labro et al. 2015). In rodents, Kv3.1b and PV are almost completely coexpressed (Weiser et al. 1995; Du et al. 1996; Chow et al. 1999; Rudy et al. 1999), whereas non-GABAergic, non-PV-immunoreactive (ir), and pyramidal Kv3.1b-ir neurons have each been observed in macaque monkey cortex (Härtig et al. 1999; Ichinohe et al. 2004; Constantinople et al. 2009; Soares et al. 2017). This suggests that primate neocortex may contain excitatory neurons capable of sustained or temporally precise high frequency firing.

The subpopulation of Kv3.1b-ir excitatory neurons includes Meynert cells (Ichinohe et al. 2004; Constantinople et al. 2009), large pyramidal neurons at the layer 5/6 border that project to area MT and the superior colliculus (Lund et al. 1975; Fries and Distel 1983; Fries et al. 1985; Nhan and Callaway 2012). The neurofilament protein (NNF-H/M) antibody SMI-32 (Sternberger and Sternberger 1983) labels a subset of pyramidal neurons in macaque V1, including Meynert cells (Campbell and Morrison 1989; Campbell et al. 1991; Hof and Morrison 1995; Chaudhuri et al. 1996; Hof et al. 1996). Recently, SMI-32 was also shown to label many Kv3.1b-ir neurons in macaque motor cortex (Soares et al. 2017).

We quantified the laminar distribution of Kv3.1b-ir, non-PV-ir, non-GABA-ir neurons in macaque V1, including the layers associated with the magnocellular (M) and parvocellular (P) pathways (Sincich and Horton 2005), and we examined whether Kv3.1b-ir, non-PV-ir neurons were generally SMI-32-ir pyramidal neurons. Sections were immunolabeled for Kv3.1b, PV, and GABA or for Kv3.1b, PV, and NNF-H/M and examined by confocal microscopy. In the GABA-labeled set of images, neurons were counted using a method that automatically identifies all DAPI-stained nuclei in a tissue volume and classifies them based on immunolabeling patterns (Kelly and Hawken 2017). Kv3.1b-ir, non-PV-ir, non-GABA-ir neuronal densities were compared with GABA-ir and PV-ir neuronal densities and with the total neuronal density in each layer. Notably, these data also allowed us to reevaluate the fraction of neurons that are GABAergic using the same measurement strategy for GABAergic and total neuronal density; this was important given that recent estimates of total neuronal density were higher than earlier measurements (Giannaris and Rosene 2012; Kelly and Hawken 2017). In the SMI-32-labeled set of images, neurons were manually identified, which allowed a comparison of the results obtained using automated counting with results obtained using a more standard approach.

Materials and Methods

Macaque V1 Tissue

Tissue samples were taken from 6 young adult male long-tailed macaque monkeys (*Macaca fascicularis*: animals M1–M5, M7) and one rhesus macaque monkey (*Macaca mulatta*; animal M6) that were used for previous anesthetized electrophysiological experiments (Cavanaugh et al. 2002; Solomon et al. 2004; Xing et al. 2004; Goris et al. 2015). After 4–6 days of recordings, experiments were terminated by intravenous injection of a lethal dose of pentobarbital (60 mg/kg), and brain death was determined by a flat electroencephalogram. Animals were perfused transcardially with heparinized 0.01 M phosphate-buffered saline (PBS, pH 7.3), followed by 4% paraformaldehyde (PFA) in 0.1 M phosphate buffer (PB, pH 7.3) (animals M1, M2, and M7) or 4% PFA plus 0.125% glutaraldehyde (animals M3–M6). Blocks of extracted brain tissue were postfixed overnight in 4% PFA at 4 °C and then serially sectioned using a vibratome. Sections from animals M3–M6 were rinsed with 1% sodium borohydride in 0.1 M PB to reduce the antigen masking effects of glutaraldehyde. All sections were immersed overnight in 30% sucrose and then stored in cryoprotectant solution at −20 °C until the time of immunohistochemical processing. For a summary of tissue preparations conducted in each animal, see Supplementary Table 1.

All experimental procedures were approved by the New York University Institutional Animal Care and Use Committee and were conducted in strict compliance with the National Institutes of Health (NIH) guidelines for the care and experimental use of animals in research.

Triple Immunofluorescence Labeling: Kv3.1b/GABA/PV

Free-floating sections were immunofluorescence stained for Kv3.1b, GABA, and PV or for SMI-32, GABA, and PV using a protocol adapted from the iDISCO method (Renier et al. 2014), excluding the final brain clearing steps, to increase penetration of antibodies into the tissue. An antigen retrieval procedure was first carried out to counteract the antigen masking effects of aldehyde fixation (Shi et al. 1991; García-Marín et al. 2013). Sections were incubated in a sodium citrate buffer solution (3.8% citric acid, 2.4% sodium citrate; pH 8.0) for 15 min in an 80 °C water bath, followed by 20 min at room temperature.

Free-floating sections were then dehydrated in 50%, 80%, and twice in 100% methanol/0.01 M PBS for 30 min each, chilled over ice, and bleached in 5% hydrogen peroxide in 20% DMSO/methanol at 4 °C overnight. They were rinsed twice in 100% methanol for 30 min each, incubated in 20% DMSO/methanol for 1 h, and rehydrated in 80%, 50%, and 0% methanol/PBS. They were incubated twice in 0.3% Triton X-100/0.01 M PBS for 30 min at room temperature, incubated for 2 h at 37 °C in 0.3% Triton X/20% DMSO/0.3 M glycine/0.01 M PBS, blocked for 2 h at 37 °C in 0.3% Triton X/10% DMSO/6% normal goat serum (NGS)/ 0.01 M PBS, rinsed twice in 0.2% Tween-20/0.01 M PBS with 10 μg/mL heparin (PTwH) for 30 min each, and incubated for 3 nights at 4 °C with rabbit anti-GABA polyclonal serum (1:1000; 20 094, Immunostar, Hudson, WI, USA). Sections were rinsed with PTwH and incubated overnight at 4 °C with Alexa Fluor® 594 goat anti-rabbit IgG (H + L) antibody (1:2000; A-11 012, Invitrogen, Carlsbad, CA, USA). The same antibody incubation steps were repeated for the remaining antibodies: mouse anti-Kv3.1b monoclonal serum (1:250; Antibodies Incorporated, Davis, CA, USA) or SMI-32 (monoclonal mouse anti-NNF-H/M; 1:4000; SMI-32 R, Covance, Emeryville, CA, USA), Alexa Fluor® 488 goat anti-mouse IgG (H + L) antibody (1:2000; A-11 001, Invitrogen), guinea pig anti-PV polyclonal serum (1:1000; 195 004, Synaptic Systems, Göttingen, Germany), and biotinylated goat anti-guinea pig IgG (1:500; BA-7000, Vector, Burlingame, CA, USA). Sections were then rinsed and incubated overnight in solution containing Alexa Fluor® 647 streptavidin conjugate antibody (1:2000; S-32 357, Invitrogen). All antibody solutions also included 3% NGS. Sections were treated according to the manufacturer's protocol with Autofluorescence Eliminator Reagent (2160, Millipore, Billerica, MA, USA) to minimize lipofuscin-like autofluorescence, counterstained with 10 μg/mL DAPI, and mounted in ProLong Gold Antifade Reagent (P-36 930, Invitrogen).

The guinea pig anti-PV antibody produces identical labeling to other PV antibodies we have used (rabbit anti-PV, Abcam, cat # AB11427; rabbit anti-PV, Swant, cat # PV-28) and matches previously published patterns of PV immunoreactivity (see Results). Detailed evaluation of the polyclonal rabbit anti-Kv3.1b antibody, prepared against a synthetic peptide corresponding to the C-terminal sequence of the Kv3.1b protein (amino acids 567–585), was described previously (Weiser et al. 1994; Constantinople et al. 2009); in immunoblots from rat (Weiser et al. 1994) and macaque (Constantinople et al. 2009) brain tissue it labeled a single band at 80–90 kDa, and preadsorption with the peptide eliminated staining (Constantinople et al. 2009). The monoclonal antibody from NeuroMAB (#75-041), prepared against a rat Kv3.1b (amino acids 437–585) fusion protein, produced identical patterns of immunolabeling to those obtained using the rabbit anti-Kv3.1b. According to

the manufacturer's technical information, this antibody labeled a single 110 kDa band in immunoblots on tissue from rat, mouse, and human brain, and labeled nothing in samples from Kv3.1/Kv3.3 double knockout mouse brain. The quality of the rabbit anti-GABA antibody (antigen: GABA coupled to BSA with glutaraldehyde) has previously been used to label GABAergic neurons in macaque cortex (Hendry et al. 1987) and was recently evaluated by Trujillo-Cenóz et al (2007) using turtle tissue. The specificity of rabbit anti-GABA was tested using a competitive inhibition ELISA, in which GABA conjugates eliminated antibody labeling, whereas glutamate, aspartate, beta alanine, tyrosine, taurine, glycine, and alanine all failed to inhibit labeling (manufacturer's technical information). Qualitatively, the pattern of GABA staining using this antibody was identical to that observed in previous studies (see Results).

Triple Immunofluorescence Labeling: Kv3.1b/SMI-32/PV

Free-floating sections were immunofluorescence stained for Kv3.1b, NNF-H/M, and PV with antibody dilutions as listed above. After the antigen retrieval procedure, sections were incubated in blocking solution (2% cold water fish skin gelatin, 1% bovine serum albumin, 2% Triton X-100, and 10% NGS in PBS), followed by overnight incubation with rabbit anti-Kv3.1b polyclonal serum (raised as described by Chow et al. 1999 and Weiser et al. 1994). Sections were incubated for 2 h at room temperature with Alexa Fluor® 594 goat anti-rabbit IgG (H + L) antibody and then overnight at 4 °C in solution containing SMI-32. Sections were incubated for 2 h with Alexa Fluor® 488 goat anti-mouse IgG (H + L) antibody, for 1.5–3 h in solution containing guinea pig anti-PV polyclonal serum, for 1 h in biotinylated goat anti-guinea pig IgG, and finally in Alexa Fluor® 647 streptavidin conjugate antibody. Autofluorescence Eliminator Reagent was used as described above. Sections were mounted in ProLong Gold Antifade Reagent.

Tissue Processing for Bright Field Microscopy

Free-floating 50 µm parasagittal sections from V1 were processed for bright field microscopy (Olympus Bx51 and Olympus VS120 microscopes, Olympus America, Center Valley, PA, USA) to examine general patterns of labeling with each primary antibody. In addition, 50 µm coronal sections through the LGN from animal M5, with initial tissue processing steps as described above for this animal, were labeled with Kv3.1b, PV, or GABA. Sections to be labeled with Kv3.1b antibodies were first treated with the sodium citrate buffer antigen retrieval procedure.

All sections were treated with 1.66% hydrogen peroxide for 30 min to remove endogenous peroxidase activity, incubated for 1 h in blocking solution (for rabbit anti-Kv3.1b: 2% cold water fish skin gelatin/1% bovine serum albumin/2% Triton X-100/10% NGS in PBS; for all other antibodies: 3% NGS/0.3% Triton X-100 in 0.01 M PBS), and then incubated 1–3 nights at 4 °C with the primary antibodies described above, diluted in the same blocking solutions. The sections were incubated overnight with biotinylated goat anti-mouse IgM (1:500; BA-2020, Vector, Burlingame, CA, USA), biotinylated goat anti-rabbit IgG (1:500; BA-1000, Vector), or biotinylated goat anti-guinea pig IgG (1:500; BA-7000, Vector). The sections were then incubated for 1 h in an avidin-biotin peroxidase complex (Vectastain ABC Elite, PK-6100, Vector) and reacted with either the Vector VIP Peroxidase Substrate kit (SK-4600, Vector) or 0.05% diaminobenzidine (DAB) plus 0.01% hydrogen peroxide in 0.01 M PBS. All treatments were followed with rinses in PBS except for the blocking step.

To enable differentiation of cortical layers when DAPI was not used, near-adjacent sections were processed for cytochrome oxidase activity using DAB as a chromagen (Seligman et al. 1968; Wong-Riley 1979; Horton 1984; Horton and Hedley-Whyte 1984). Sections were incubated overnight at 37 °C in a solution containing 0.03% cytochrome c, 0.02% catalase, and 0.05% DAB in 0.1 M PB.

Sections were slide-mounted, dehydrated in ethyl alcohol, cleared with xylene, and coverslipped.

Confocal Microscopy

Fluorescence sections were imaged using a Leica TCS SP5 confocal system (Leica Microsystems, Wetzlar, Germany). A 488 nm Argon laser, a 561 nm DPSS laser, a 633 nm HeNe laser, and a 405 nm diode laser were used to excite the Alexa Fluor 488, 594, and 647 fluoresceins and DAPI, respectively. Gain and offset levels for channels with strong signal to noise (DAPI, SMI-32, PV) were set such that bright labeled regions were at saturation and there was minimal background fluorescence. For channels with lower signal to noise (GABA, Kv3.1b), gain and offset levels were set to preserve the range of intensity levels: few pixels were allowed to saturate, and only regions within blood vessels or above the pial surface fell under the low intensity offset level. Image stacks were acquired by specifying an upper and lower z position and acquiring each channel sequentially, using a 63× oil-immersion objective lens (NA 1.4, refraction index 1.45), and a pinhole size of 1 airy unit. The scanning speed was 200 Hz, the z step size was 0.5 µm, and the (x–y) image resolution per frame was 1024 × 1024 pixels (246.03 µm × 246.03 µm) with no digital zoom applied.

Samples were from the dorsal opercular surface of V1 (expected eccentricity 2–5 degrees). A strip of tissue was selected that had consistent labeling quality and no tears across the vertical span from the pial surface to white matter. A series of z stacks was acquired, beginning with a stack that included the pial surface and subsequently moving towards the white matter such that each sequential volume overlapped slightly in the y dimension and as completely as possible in the x dimension (Fig. 1). The final stack contained the layer 6/white matter boundary. The mean cortical depth (y extent) was 1.40 mm ± 0.05 mm (mean ± SEM, n = 23) for the Kv3.1b/GABA/PV-labeled set of image series and 1.48 mm ± 0.04 mm (mean ± SEM, n = 11) for the Kv3.1b/SMI-32/PV-labeled set. Gain and offset levels were constant across images within a series.

The total thickness (z distance) sampled from each animal was greater than 20 µm after removing excluded regions and correcting for tissue shrinkage. For Kv3.1b/GABA/PV image stacks, the upper image stack z limit was just "above" (closer to the objective lens) the cut surface of the tissue, and the lower z limit was several µm below the limit of antibody penetration. The set included 23 series, with 6–11 series from each animal. After every second z stack, the DAPI channel was imaged with a 1 µm z step in a stack with z limits specified above and below the cut surfaces of the tissue; this was used to measure tissue shrinkage in the z dimension. For Kv3.1b/SMI-32/PV image stacks, z limits were specified to maximize the volume acquired without sampling regions beyond the range of antibody penetration. The set included 11 series, with 3–4 series from each animal.

Cell Counting: Kv3.1b/GABA/PV

DAPI images were automatically analyzed using a previously described method that identifies 3D centroid positions of all
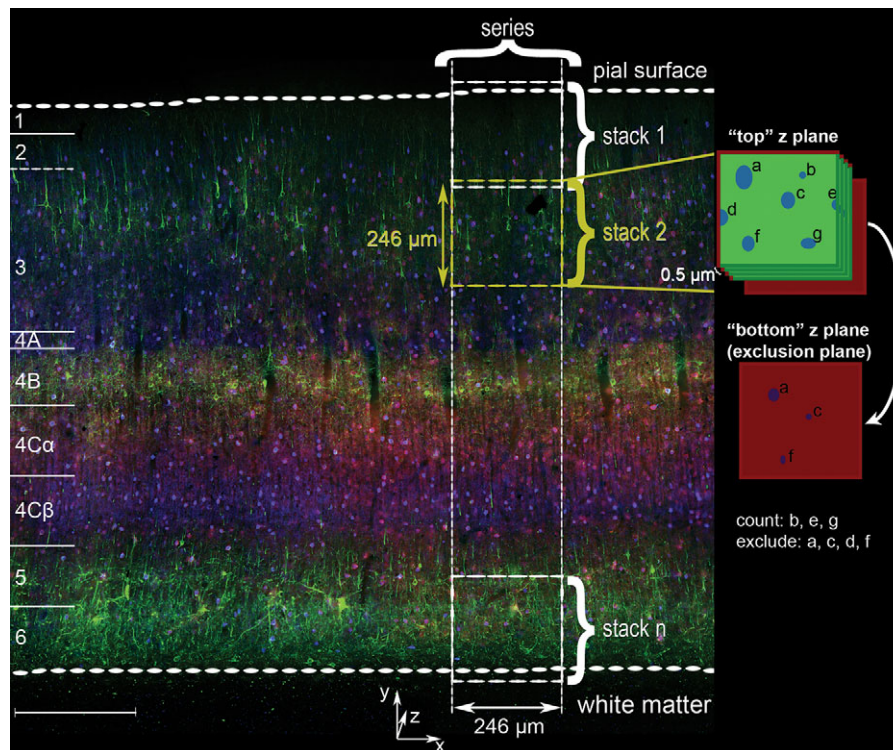
Figure 1. Overview of PV, Kv3.1b, and SMI-32 coimmunoreactivity in macaque V1 with schematized sampling organization and counting criteria. Micrograph of triple immunofluorescence labeled tissue from animal M2 acquired using an Olympus VS120-FL scanning system. Cortical layers indicated at far left. Green: SMI-32; red: Kv3.1b; blue: PV. Scale bar: 300 μm. Right: a series of confocal z stacks was acquired such that each stack overlapped slightly in the y dimension with the previous and subsequent stacks, and the full set of z stacks in each series spanned the depth of cortex from the pial surface to white matter. Far right: implementation of exclusion boundaries (red edges and bottom plane) used for the manual counting of the SMI-32-labeled set of image series were defined according to stereological criteria. Cells were excluded from quantification if they intersected either of the left or upper edges of an individual counting frame, as well as if they were still visible in the lowest z plane in the stack. In this idealized example, cells b, e, and g would have been counted, while a, c, d, and f would have been excluded.

nuclei in each image stack (Kelly and Hawken 2017). The sets of nuclei were restricted using stereological exclusion boundaries (Sterio 1984; Gundersen et al. 1988); each z stack was treated as a 3D counting brick probe (Howard et al. 1985; Williams and Rakic 1988). Any object that intersected the farthest rightward or lowest edge of an image was excluded. Cells were also excluded if their centroids fell above a user-specified upper z plane or fell at or below a lower z plane boundary. The upper boundary was 4 z planes below the cut surface of the tissue (a 2 μm guard region). The lower boundary was determined by identifying the limit of antibody penetration for each antibody in each z stack, finding the minimum usable z distance across all stacks, and subtracting that distance from the upper boundary of each stack. Thus, the same volume was sampled in every image stack from a given series. Finally, cells were eliminated if their centroids fell within the region of overlap with the subsequent image stack.

The remaining DAPI-labeled nuclei were classified by determining whether there was immunolabeling for any combination of the 3 antigens at the centroid location. Binary mask images were generated for each channel (Supplementary Fig. 1). In the nearest z plane to each DAPI centroid, each channel's mask image was evaluated within a circular region two-thirds the radius of the corresponding DAPI profile. If at least 90% of pixels in this region were foreground, the object was classified as labeled by the corresponding antibody. Classification errors were corrected manually as follows. For each channel, the positions of 3D centroids classified as labeled and unlabeled in that channel

were plotted at their nearest z planes on the original micrographs. Visually identified errors were marked using the Cell Counter plugin by De Vos for ImageJ (Schneider et al. 2012). Marker positions were imported into MATLAB and matched to their nearest centroids; the classification of each marked cell for that channel was reversed.

For Kv3.1b, cells were considered labeled if a continuous ring was present around the soma in the apparent location of the cell membrane, and if this signal could not be predicted by the presence of PV-ir processes or axon terminal boutons. In instances of unresolvable uncertainty, cells were categorized as non-ir. For PV and GABA, cells were categorized as ir if they contained any discernable somatic staining. These criteria were intended to minimize false positive identification of Kv3.1b-ir, non-PV-ir, non-GABA-ir neurons.

Cell Counting: Kv3.1b/SMI-32/PV

Cells were counted manually using the ImageJ Cell Counter plugin by placing markers at the approximate center of the cell. Stereological exclusion boundaries were implemented as schematized on the right side of Figure 1. Cells were excluded if their somata intersected the lowest z plane in each stack; if they intersected the upper or left edges of the counting frames (exclusion edges); and/or if they were within the region of overlap with the previous stack.

Identified cells were categorized by their combined pattern of immunoreactivity for each antigen (i.e., "SMI-32-ir only,"

"PV-ir-only," "SMI-32- and Kv3.1b-ir only," etc.). Neurons were considered SMI-32-ir if they contained labeling that was distinct from the background signal, regardless of intensity.

Computing Laminar Densities and Density Profiles

To measure the distribution of each category of neuron, the position of each included cell was converted to distance from the pial surface, accounting for the y position of the pial surface in the uppermost counting volume and the cumulative overlap in the y dimension between successive z stacks. These distances were converted to relative cortical depth (relative cortical depth = cell depth / white matter depth) and binned (2.5% of total cortical depth per bin).

For each monkey, counts within each bin were summed, as were bin volumes (corrected to account for tissue shrinkage) across samples from that animal. The summed counts were divided by the summed volume to produce an average density profile across relative cortical depth for each animal. Across animals, the average density profile was the mean of the 3 animals' density profiles.

Tissue shrinkage in the z dimension was quantified by measuring the distance from the top to the bottom of the mounted tissue (mean distance, Kv3.1b/GABA/PV set: 37.2 μm ± 1.5 μm SEM, $n = 23$; Kv3.1b/SMI-32/PV set: 38.6 μm ± 1.4 μm SEM, n = 11) and comparing this to the 50 μm thickness at the time of sectioning. For the GABA/Kv3.1b/PV set, shrinkage in x and y was also estimated for each series by identifying the same blood vessels in the processed section and in an image of the same section acquired prior to immunolabeling using an Olympus VS120-FL virtual slide scanning system (Olympus America, Center Valley, PA, USA). The extent from the pial surface to the white matter (y length) at the locations of blood vessel landmarks and the horizontal (x) lengths between landmarks at the level of the stria of Gennari were measured in local regions surrounding the sampled sites. Across samples, the mean shrinkage in x was 16%, while the mean shrinkage in y was 12%; that is, the original size in the x dimension was 1.19 times the size after processing, while the original size in the y dimension was 1.14 times the size after processing. Tissue shrinkage in the x and y dimensions was not measured in the SMI-32/Kv3.1b/ PV set.

Densities of each type of neuron were similarly computed within each cortical layer. Laminar boundaries were identified separately for each sampled image series. Layers of area V1 were defined according to Brodmann (1909) nomenclature, modified by Lund (1973). This system distinguishes 4 subdivisions of layer 4: 4 A, 4B, 4 Cα, and 4 Cβ. In the SMI-32-labeled set, laminar boundaries were identified in immunofluorescence labeled material and, when possible, confirmed using adjacent cytochrome oxidase stained sections. In the GABA-labeled set, boundaries were identified based on transitions in density of DAPI-labeled nuclei and the pattern of neuropil staining by anti-PV (Van Brederode et al. 1990; Disney and Reynolds 2014).

Each cell type was also considered as a fraction of the total neuronal population. Because the automated analysis method used to count GABA-ir, PV-ir, and Kv3.1b-ir neurons was previously used to measure total neuronal density in NeuN-labeled V1 tissue (Kelly and Hawken 2017), the densities of the overall DAPI-labeled cell population could be directly compared with the previously reported values. The DAPI-labeled cell densities in the GABA/Kv3.1b /PV set (Supplementary Table 2) were remarkably consistent with the densities measured in the NeuN-labeled tissue (García-Marín et al. 2017), so neuronal densities were estimated as a proportion of the total cell density within each layer. For SMI-32-labeled tissue, which was not labeled with DAPI, densities were compared with the previously reported neuronal densities (García-Marín et al. 2017; Supplementary Table 2).

Image Processing for Figures

Micrographs presented in figures were captured using an Olympus Bx51 light microscope with an Olympus Microfire digital camera (Olympus America), a Leica TCS SP5 confocal system, or an Olympus VS120-FL virtual slide scanning system. ImageJ was used to generate maximum intensity z projections and to adjust image brightness and contrast. Figures were produced in Adobe Photoshop CS and Adobe Illustrator CS (Adobe Systems, San Jose, CA, USA).

Results

Classifying Neurons by Kv3.1b, GABA, PV, and NNF-H/M Expression

Patterns of subcellular localization and laminar variations in immunoreactivity (Figs 1 and 2, Supplementary Fig. 2) were consistent with previously described patterns (e.g., Fitzpatrick et al. 1987; Hendry et al. 1987; Van Brederode et al. 1990; Beaulieu et al. 1992; Hof and Morrison 1995; Constantinople et al. 2009). Each antigen was expressed within the somata or in the somatic membranes of subsets of V1 neurons, allowing classification of neurons based on inspection of somata. Labeling with both anti-GABA (Fig. 2A, D) and anti-PV (Fig. 2B, E, H, K) appeared diffuse throughout labeled somata. SMI-32 stained the perikaryal regions of somata and the dendritic arbors of labeled neurons (Fig. 2G, J). The Kv3.1b subunit was concentrated most heavily in cell membranes associated with somata and occasionally proximal processes (Weiser et al. 1995; Du et al. 1996; Härtig et al. 1999; Hernández-Pineda et al. 1999), although some signal was also present in the cytoplasm just inside the cell membrane. This pattern was the same using both Kv3.1b antibodies (Fig. 2C, F, I, L).

Neurons were categorized by their combined patterns of immunoreactivity for multiple antigens. In the Kv3.1b/GABA/PV set, neurons that were PV-ir were often also GABA-ir and Kv3.1b-ir (Fig. 2A–F, arrowheads), but many neurons expressed only GABA (Fig. 2A–F, arrows) or only Kv3.1b (Fig. 2A–F, asterisks). In the Kv3.1b/SMI-32/PV set, neurons displayed multiple coexpression patterns, including: immunoreactivity only for Kv3.1b (Fig. 2G–I, asterisk), PV, or SMI-32; immunoreactivity for both Kv3.1b and PV but not SMI-32; immunoreactivity for both Kv3.1b and SMI-32 but not PV (Fig. 2J–L, arrows); and coimmunoreactivity for all 3 antigens (Fig. 2G–L, arrowheads).

Inhibitory to Excitatory Neuron Ratio

Because the macaque monkey is a commonly studied primate model that can be used to identify species-specific features of cortical circuitry, it was important to accurately establish the frequency of specific cell types relative to the overall neuronal population, including the proportion of inhibitory to excitatory neurons. Previous studies reported that inhibitory interneurons account for 15–20% of the total neuronal population in macaque V1 and about 25% of the total population in extrastriate cortex (Fitzpatrick et al. 1987; Hendry et al. 1987; Beaulieu et al. 1992). However, recent studies (Giannaris and Rosene 2012; Kelly and Hawken 2017; García-Marín et al. 2017; Supplementary Table 2) have shown that total neuronal density in macaque V1 is about
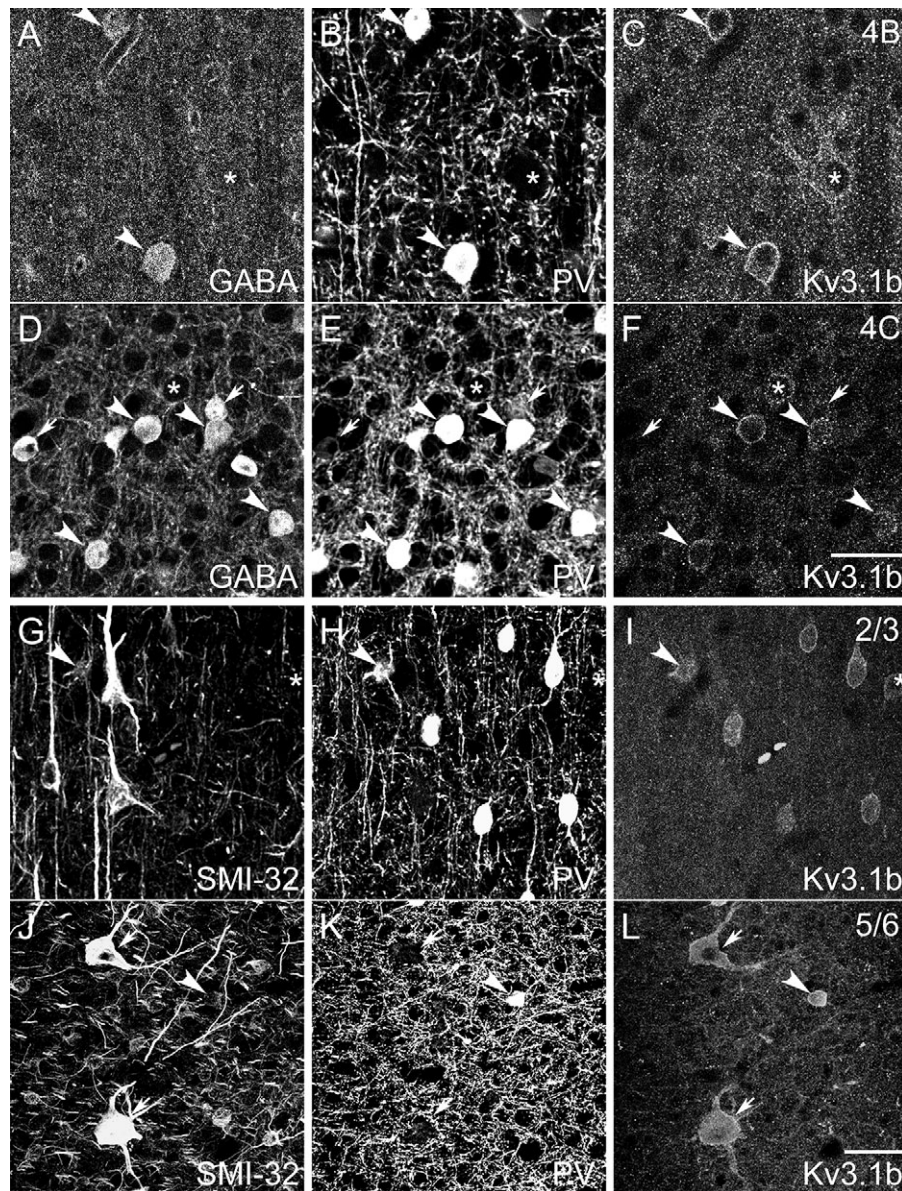
Figure 2. Confocal micrographs of tissue triple immunofluorescence labeled with GABA (*A, D*), anti-PV (*B, E, H, K*), mouse anti-Kv3.1b (*C, F*), SMI-32 (*G, J*), and rabbit anti-Kv3.1b (*I, L*). (*A–F*): Confocal micrographs from layers 4B (*A–C*) and 4 C (*D–F*) of animals M6 and M5, respectively, reveal that neurons expressed various combinations of GABA, PV, and Kv3.1b. Images are single confocal image planes. Arrows: neurons ir only for GABA. Asterisks: neurons ir only for Kv3.1b. Arrowheads: neurons ir for all 3 antigens. Scale bar in *F* (refers to *A–F*): 25 μm. (*G–L*): Example neurons labeled for SMI-32, PV, and Kv3.1b in a parasagittal section from layer 2/3 of animal M1 (*G–I*) and in a horizontal section from layer 5/6 of animal M7 (*J–L*). Images are maximum projections of z stacks, with z lengths of 5.0 (*G–I*) and 4.5 (*J–L*) μm. Examples include neurons ir for SMI-32 and Kv3.1b but not for PV (arrows); a neuron ir only for Kv3.1b (asterisk); and neurons ir for all 3 antigens (arrowheads). Note the 2 Meynert cells in (*J–L*) (arrows). Scale bar in *L* (refers to *G–L*): 25 μm (*G–I*), 50 μm (*J–L*).

twice as high as previously estimated (O'Kusky and Colonnier 1982; Beaulieu et al. 1992). Therefore, it was essential to reevaluate whether GABAergic cell densities were also higher than previously reported or whether the proportion of inhibitory neurons within the total neuronal population was lower than the previously accepted values.

In macaque V1, GABA-ir neurons were present in all layers (Fig. 3A, Supplementary Fig. 2A; Supplementary Table 3), with densities corresponding to 6–14% of the total neuronal population in layers 2–6, depending on cortical depth (Fig. 3B). The average fraction of neurons that were GABAergic across all layers of V1, 11%, was considerably lower than measured in previous studies (Fitzpatrick et al. 1987: 15%; Hendry et al. 1987:

20%; Beaulieu et al. 1992: 21%). The density of GABAergic neurons was similar to previously reported values; the difference in proportion of GABAergic neurons reflected higher total neuronal densities (Kelly and Hawken 2017). In layer 1, a majority of the neuronal population was GABA-ir, which is qualitatively consistent with previous observations (Fitzpatrick et al. 1987; Hendry et al. 1987; Beaulieu et al. 1992).

Laminar Densities of PV-, Kv3.1b-, and SMI-32-ir Neurons

PV-ir neurons were present throughout layers 2–6 (Fig. 4A, Supplementary Fig. 3A; Supplementary Table 3), with the highest
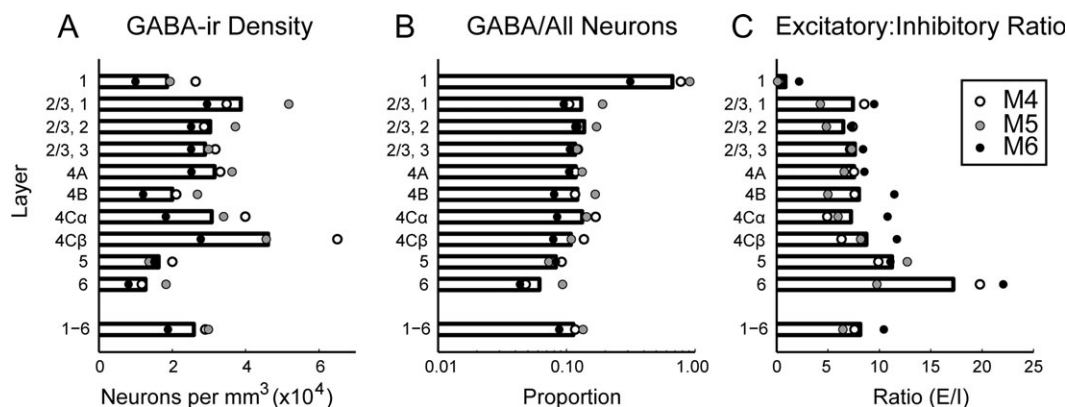
Figure 3. Absolute and relative density of GABA-ir neurons in each cortical layer. (A): Density per mm^3 of GABA-ir neurons computed within laminar boundaries specified separately for each image series. Bars show mean across animals; average laminar densities from each animal are plotted as points. (B): Proportion of all neurons in each layer (García-Marín et al. 2017) that were GABA-ir. (C): Ratio of non-GABA-ir to GABA-ir neurons in each layer. Density of non-GABA-ir neurons was computed by subtracting the GABA-ir neuronal density measured in this study from the total neuronal density, which was estimated by multiplying the total DAPI-labeled cell density by the ratio of neurons to all cells in each layer reported previously (García-Marín et al. 2017).

density in layer 4 Cβ. There were more PV-ir neurons in 4 Cβ than in 4 Cα, consistent with the previous observations (Blümcke et al. 1990). PV-ir neurons were relatively infrequent in layers 5 and 6 and were not observed in layer 1 (Fig. 4A). A dearth of PV-expressing neurons in layer 1 is consistently observed across studies (Celio 1986; Van Brederode et al. 1990; Disney and Reynolds 2014).

Kv3.1b-ir somata were similarly distributed throughout layers 2–6 (Fig. 4B, Supplementary Fig. 3B; Supplementary Table 3). Because we identified as Kv3.1b-ir only those neurons that could be classified with certainty, the reported densities are likely a lower bound on the true density of Kv3.1b-expressing neurons in V1. The distribution of cell densities across cortical depth and layers was well matched between the 2 independent estimates (Kv3.1b/PV/GABA and Kv3.1b/PV/SMI-32), despite the different animals, tissue processing protocols, and counting methods used. However, the absolute densities of Kv3.1b-ir neurons and PV-ir neurons measured from the Kv3.1b/PV/GABA-labeled tissue (Fig. 4; Supplementary Table 3) were lower than the absolute densities measured from the Kv3.1b/PV/SMI-32-labeled tissue (Supplementary Fig. 3; Supplementary Table 4) by 14 and 13%, respectively. This can be attributed to tissue shrinkage in the x and y dimensions that was measured and corrected for only in the GABA-labeled set. The densities measured from the 2 sets would be matched if the tissue samples used in the second set shrunk by 6% in each of the x and y dimensions. Neuropil staining for Kv3.1b was densest in layers 4 C and 4B (Supplementary Fig. 2B).

The labeling intensity of SMI-32-ir neurons varied (Supplementary Figs. 2D, 4). Neurons with SMI-32-ir apical and proximal basal dendrites often showed more intense staining in the dendrites compared to somata (Supplementary Fig. 4A). The most intensely labeled neurons were the Meynert-Cajal cells (Hof et al. 1996, 2000) in layer 4B (Supplementary Fig. 4B) and the Meynert cells (Supplementary Fig. 4E). SMI-32-ir neuronal densities (Fig. 4C; Supplementary Table 4) were highest in layer 6 (Supplementary Fig. 4D–F) and in the middle third of layers 2/3. Our estimate of SMI-32-ir neuronal density in the lower two-thirds of layer 2/3 (46 800 neurons/mm^3) was quite close to the previously reported 53 691 SMI-32-ir neurons per mm^3 in layer 3 (Hof and Morrison 1995). In contrast, our estimate of SMI-32-ir density across layers 5 and 6 (47 900 neurons/mm^3) was

more than double the previous estimate (20 341 neurons/mm^3; Hof and Morrison 1995), possibly due to the immunocytochemical methods or criteria used in the 2 studies. More sensitivity for SMI-32 immunoreactivity may have given rise to the labeling and inclusion of some of the more faintly labeled somata (Supplementary Fig. 4D, thick arrow); most layer 6 neurons identified as SMI-32-ir in the present study were relatively small and lightly labeled. This might also be the reason we observed neurons in layer 4 C (Supplementary Fig. 4C), while others have reported a dearth of SMI-32-ir neurons in this layer (Campbell and Morrison 1989; Chaudhuri et al. 1996; Hof et al. 1996; Soares et al. 2008). SMI-32-ir neurons have previously been observed in layer 4 C (Fenstemaker et al. 2001).

Coexpression of PV with GABA

Across all layers, almost all PV-ir neurons were also GABA-ir (96% of all PV-ir neurons); PV-ir neurons can be considered a subset of the GABAergic population. The proportion of GABA-ir neurons that were also PV-ir varied across cortical depth (Fig. 5). Across all layers, the proportion of GABA-ir neurons that were PV-ir in this study (52%) was lower than previously reported in macaque V1 (74%; Van Brederode et al. 1990). Only 42% of GABA-ir neurons were PV-ir in layer 2/3, where there are substantial populations of calbindin (CB)- and calretinin (CR)-expressing interneurons (Van Brederode et al. 1990; Kondo et al. 1994; Morrison et al. 1998; DeFelipe et al. 2006). The proportion of GABA-ir neurons that were coPV-ir was highest in layer 4 C (4 Cα: 80%, 4 Cβ: 78%), again lower than the proportion (nearly 100%) reported by Van Brederode et al. (Van Brederode et al. 1990). Figure 2D–F includes several examples of neurons in layer 4 C that are clearly GABA-ir but show no immunoreactivity for PV (arrows).

Coexpression of Kv3.1b with GABA and PV

Laminar densities of neurons with all possible combinations of GABA, PV, and Kv3.1b immunoreactivity are presented in Supplementary Table 3. PV and Kv3.1b were frequently coexpressed, as previously observed in rodents (Weiser et al. 1995; Du et al. 1996; Chow et al. 1999; Rudy et al. 1999) and primates
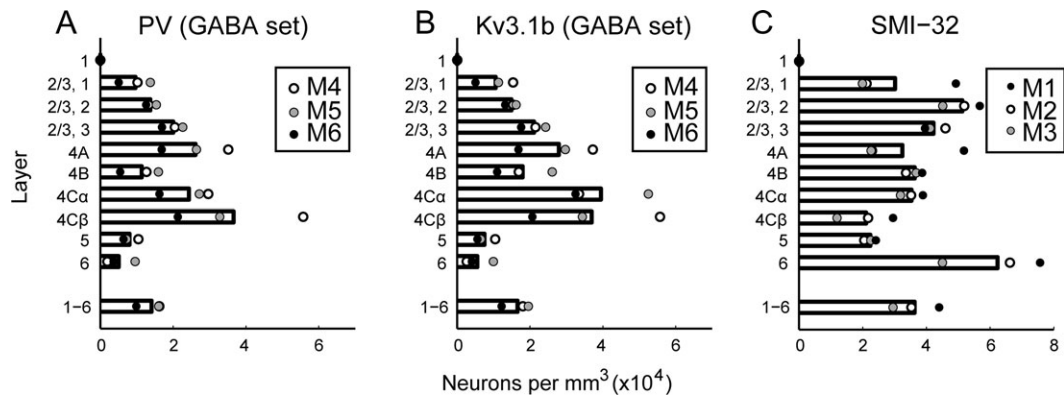
Figure 4. Density distributions of PV-ir, Kv3.1b-ir, and SMI-32-ir neurons in V1. Density per mm^3 of PV-ir (A), Kv3.1b-ir (B), and SMI-32-ir (C) neurons computed within laminar boundaries specified separately for each image series. Bars show mean across animals; average laminar densities from each animal are plotted as points. Estimates of PV-ir and Kv3.1b-ir neuronal densities are from GABA-labeled sections.
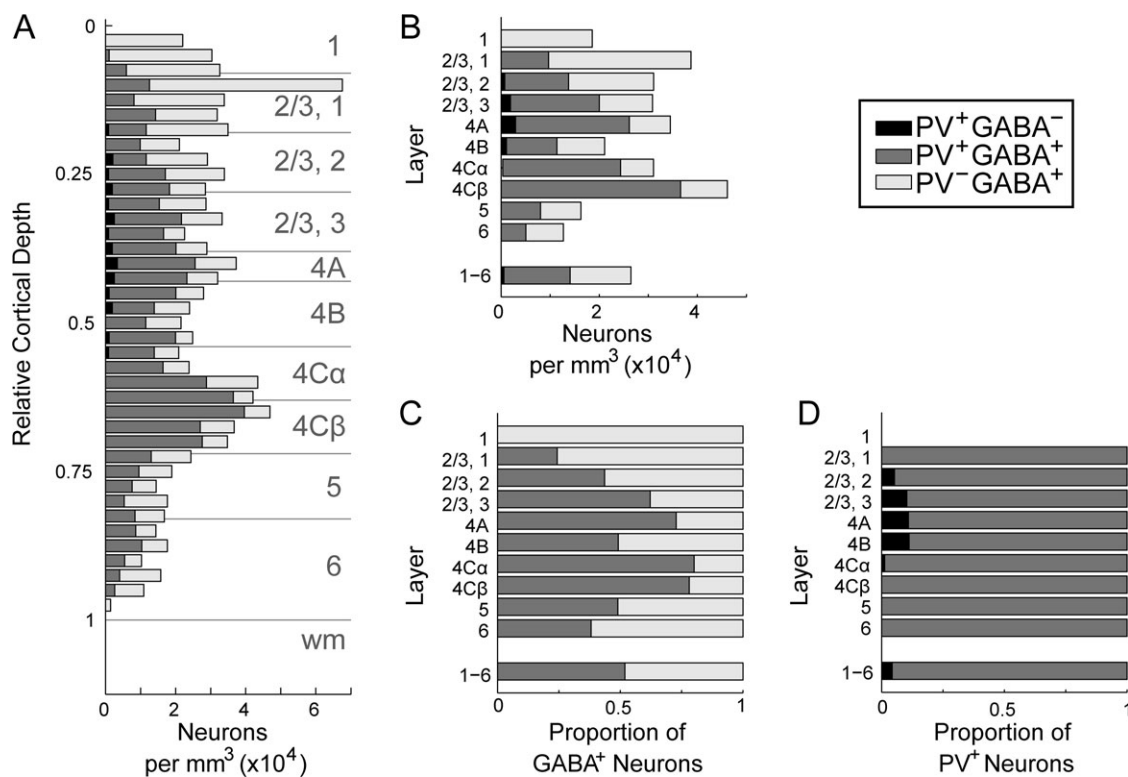

Figure 5. Coexpression of PV and GABA in V1. Data from animals M4-M6. (A): Density (×10^4) per mm^3 of neurons ir for GABA (light gray), PV (black), or both (dark gray) as a function of relative cortical depth. Depths (y positions) were converted to relative cortical depth and binned with a bin size equal to 2.5% of total cortical depth. The number of neurons in each bin was divided by the tissue volume per bin, yielding the distribution of neurons across cortical depth. (B): Density per mm^3 of each neuron type computed within laminar boundaries specified separately for each image series. (C): Proportion of GABA-ir neurons in each cortical layer accounted for by GABA-ir, PV-ir (dark gray) and GABA-ir, non-PV-ir (light gray) neurons. (D): Proportion of PV-ir neurons in each cortical layer accounted for by PV-ir, GABA-ir (dark gray) and PV-ir, non-GABA-ir (black) neurons.

(Ichinohe et al. 2004; Constantinople et al. 2009; Soares et al. 2017). Across all layers, 79–80% of Kv3.1b-ir neurons were also PV-ir (478 of 603 neurons, GABA-labeled set; 452 of 571 neurons, SMI-32-labeled set), and 94% of PV-ir neurons were also Kv3.1b-ir (478 of 507 neurons, GABA-labeled set; 452 of 480 neurons, SMI-32-labeled set). These results are concordant with those of Constantinople et al (2009). Of the Kv3.1b-ir, PV-ir neurons in the GABA-labeled series, only 4% had no discernable GABA immunoreactivity (20 of 478 neurons).

Although PV-ir neurons comprised only 52% of the total GABA-ir population, they comprised nearly the entire subset of Kv3.1b-ir GABAergic neurons. Considering only neurons ir for Kv3.1b, 96% of PV-ir neurons across all cortical layers were also GABA-ir, and 99% of GABA-ir neurons were also PV-ir. Only a minor subset of cells was both GABA-ir and Kv3.1b-ir but not PV-ir. These cells may have been CB-ir, Kv3.1b-ir neurons, as described previously (Constantinople et al. 2009); if so, they were less frequently observed in our samples.
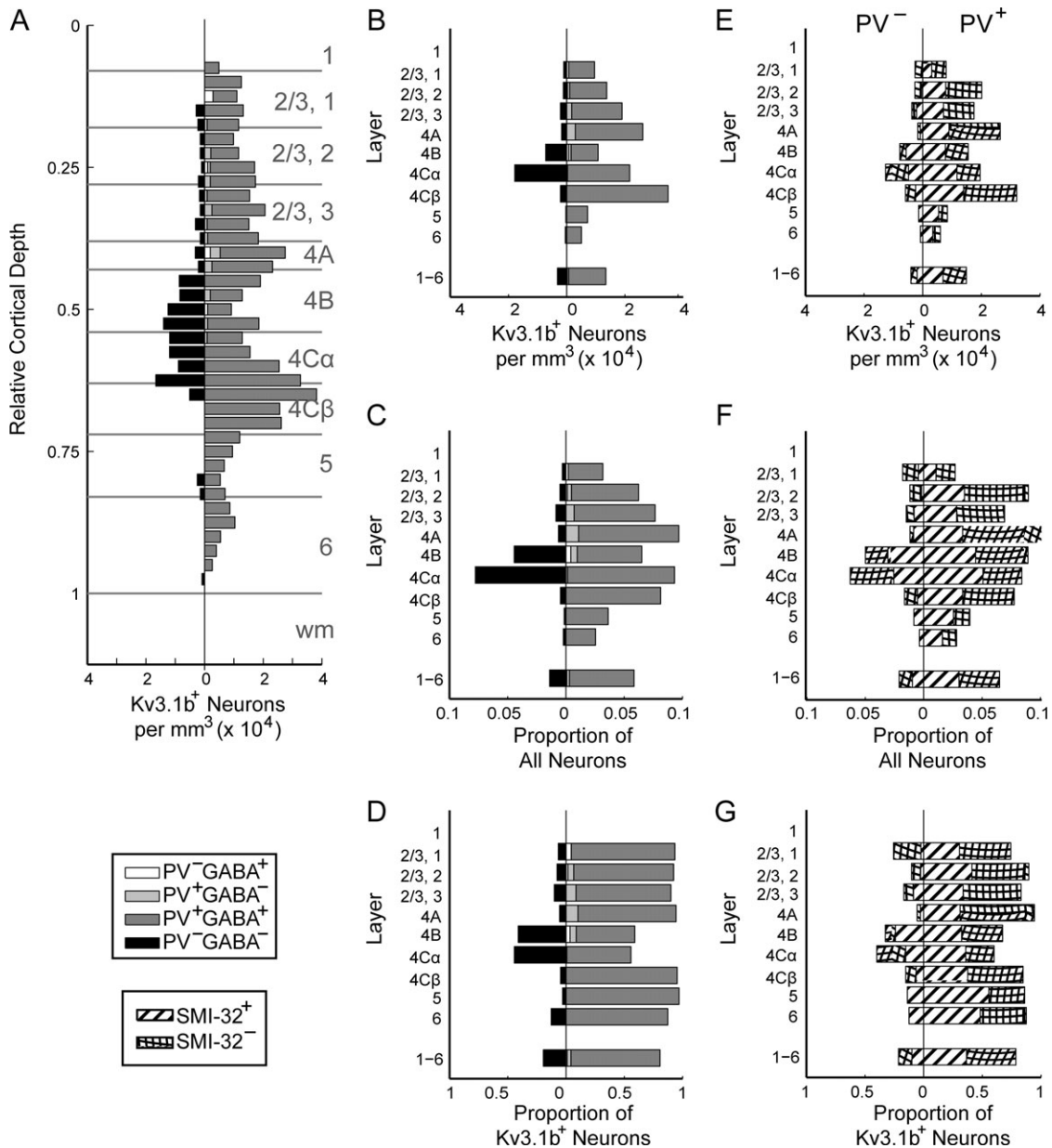
Figure 6. Density distributions of Kv3.1b-ir neurons by coimmunoreactivity. Data from animals M4-M6. (A): Density per mm³ of Kv3.1b-ir, non-GABA-ir, non-PV-ir neurons (black; left of vertical); Kv3.1b-ir, GABA-ir, non-PV-ir (white; right of vertical); Kv3.1b-ir, PV-ir, non-GABA-ir (light gray; right of vertical); and Kv3.1b-ir, GABA-ir, and PV-ir (dark gray; right of vertical) as a function of relative cortical depth. (B): Densities of neurons of each type (types as in A) in each cortical layer. (C): Frequency of neurons by type (types as in A) relative to the total neuronal population in that layer (García-Marín et al. 2017). (D): Frequency of neurons by type (types as in A) relative to the total Kv3.1b-ir neuronal population in that layer. (E): Densities of Kv3.1b-ir neurons that were (right) and were not (left) also ir for PV in each cortical layer. Bars filled with striped pattern represent neurons that were also SMI-32-ir, while bars filled with hatched pattern represent neurons that were not SMI-32-ir. (F): Proportion of total neuronal population in each layer accounted for by each type of neuron (types as in E). (G): Frequency of each type of Kv3.1b-ir neuron (as in E) relative to total Kv3.1b-ir population.

Kv3.1b Expression in non-GABA-ir Neurons

A substantial subpopulation of Kv3.1b-ir neurons was neither PV-ir nor GABA-ir (Fig. 6), in contrast to observations in rodent cortex (Chow et al. 1999; Rudy et al. 1999; Rudy and McBain 2001). Axons of PV-ir GABAergic neurons establish basket formations surrounding the cell bodies of many excitatory neurons. Although it would be surprising for only a small subset of excitatory cells to be surrounded by dense Kv3.1b-ir baskets, it was important to distinguish staining of basket terminals from staining of the excitatory cell membrane itself. Higher-resolution

confocal images show a very similar pattern of Kv3.1b staining in Kv3.1b-ir, non-PV-ir neurons (Fig. 7, asterisks) and in Kv3.1b-ir, PV-ir neurons (Fig. 7, arrowheads), appearing as continuous ring-like staining through the cell membrane in single z planes, consistent with previous observations (Härtig et al. 1999; Constantinople et al. 2009). Many Kv3.1b-ir, non-PV-ir neurons appeared to be surrounded by a basket of PV-ir terminals (e.g., Fig. 7, arrows), but this was distinct from the membrane staining that continued through the regions between PV-ir puncta. A cell was classified as Kv3.1b-ir only if there was a clear ring of staining that could not be explained by a punctate ring of PV label, and at least part of
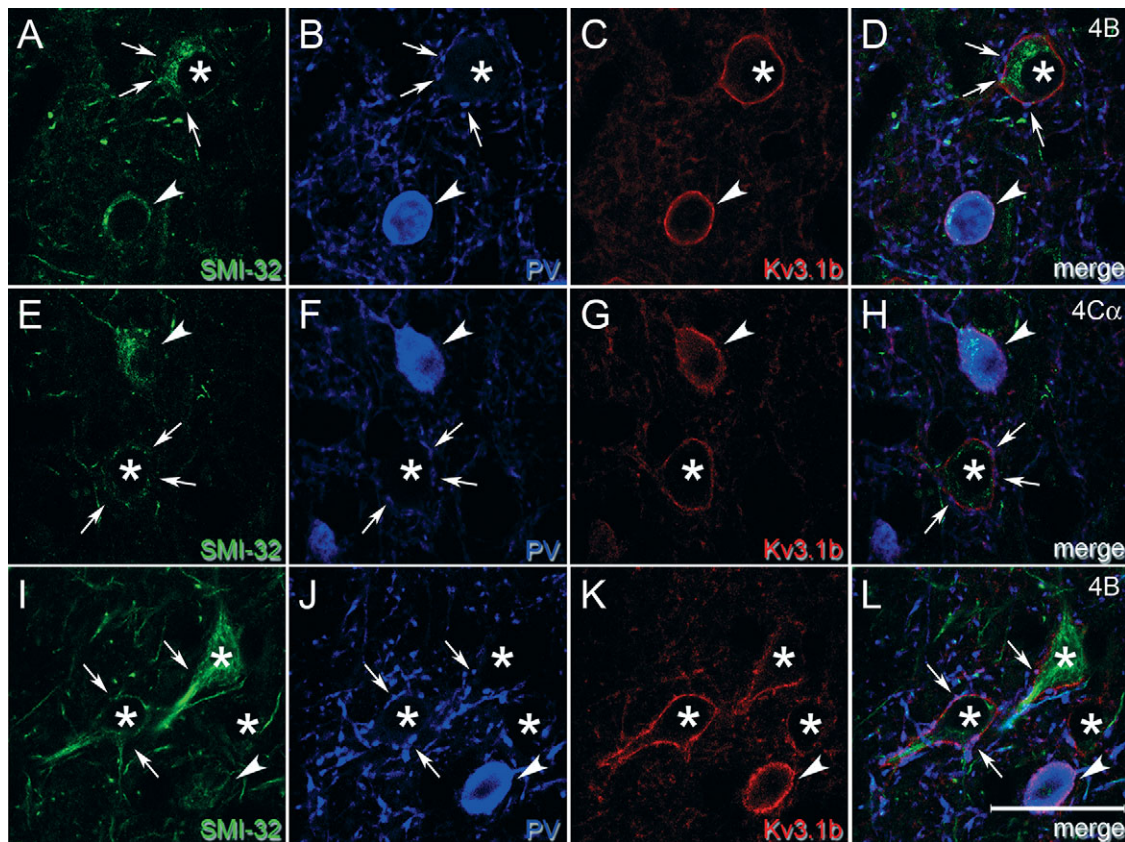
Figure 7. High magnification images compare cell membrane staining of Kv3.1b in PV-ir and non-PV-ir neurons. Single z plane images from sampled regions in layer 4B (*A–D, I–L*) and 4Cα (*E–H*) of animal M1. These regions contained neurons that were both Kv3.1b-ir and PV-ir (arrowheads) and neurons that were Kv3.1b-ir but not PV-ir (asterisks). Although the Kv3.1b-ir, non-PV-ir neurons appeared to be surrounded by perisomatic baskets of PV-ir terminals, some of which are indicated by arrows, there was also continuous membrane Kv3.1b staining apparent in the intervening regions. At least 2 of these Kv3.1b-ir, non-PV-ir neurons—asterisk in *I–L*—had the shape of pyramidal cells and were SMI-32-ir. Scale bar: 25 μm.

which appeared to be closer to the center of the neuron compared to surrounding PV staining.

About one-fifth of Kv3.1b-ir neurons were neither PV-ir nor GABA-ir, and this subset of neurons was non-uniformly distributed across cortical depth (Fig. 6A, left of vertical). For comparison, the densities of Kv3.1b-ir neurons that were also PV-ir and/or GABA-ir are also plotted at each depth (Fig. 6A, right of vertical). The density of ir neurons in each layer (Fig. 6B) was divided by the total neuronal density in that layer to obtain the proportion of each neuron type relative to all neurons in that layer (Fig. 6C; parentheses in Supplementary Table 3). Kv3.1b-ir neurons of each type were also considered as a fraction of all Kv3.1b-ir neurons in each layer (Fig. 6D). The densities of excitatory Kv3.1b-ir neurons in layers 4Cα and 4B were almost as high as the densities of inhibitory Kv3.1b-ir neurons. The proportions of Kv3.1b-ir neurons that were non-PV-ir were similar in the GABA-labeled (20%) and SMI-32-labeled tissue (21%), despite the use of different Kv3.1b antibodies, tissue processing protocols, and counting methods.

The density of Kv3.1b-ir, non-PV-ir, non-GABA-ir neurons was highest in layers 4B and 4Cα, both of which are M pathway dominated. 41% of all Kv3.1b-ir neurons in layer 4B and 44% of Kv3.1b-ir neurons in layer 4Cα were non-PV-ir and non-GABA-ir. In the SMI-32-labeled set, 33% of Kv3.1b-ir neurons in layer 4B and 40% of Kv3.1b-ir neurons in layer 4Cα were non-PV-ir. In layer 4B and layer 4Cα, respectively, 4% and 8% of the estimated total neuronal population were Kv3.1b-ir but neither PV-ir nor GABA-ir. In contrast, in P pathway dominated layer 4Cβ, merely 1% of the total neuronal population was Kv3.1b-ir and non-PV-ir.

In layer 2/3, 11% of Kv3.1b-ir neurons were non-PV-ir (17% in the SMI-32-labeled set). Layers 2 and 3 contain non-PV-ir inhibitory interneurons that express other markers, such as CB (Van Brederode et al. 1990) and CR (Meskenaite 1997), but the majority (86%) of Kv3.1b-ir, non-PV-ir neurons were also non-GABA-ir in layer 2/3. In layers 5 and 6, most (93% in the GABA-labeled set; 87% in the SMI-32-labeled set) Kv3.1b-ir neurons were also PV-ir, and all Kv3.1b-ir, non-PV-ir neurons identified in the GABA-labeled set were also non-GABA-ir. The Kv3.1b-ir, non-PV-ir, non-GABA-ir population in layers 5/6 included the Meynert cells and smaller cell types. The densities of Kv3.1b-ir, PV-ir and Kv3.1b-ir, non-PV-ir neurons were similar in both studies, with the exception of a slightly higher frequency of Kv3.1b-ir, non-PV-ir neurons in layer 2/3 in the SMI-32-labeled set.

Coexpression of Kv3.1b and SMI-32

Many, but not all, Kv3.1b-ir, non-PV-ir neurons coexpressed SMI-32-labeled NNF-H/M proteins (Fig. 2). Figure 6E–G distinguishes the Kv3.1b-ir, non-PV-ir neurons (left of center) that were (striped) and were not (hatched) SMI-32-ir. Dividing the density of SMI-32-ir neurons by the average overall density of neurons

in V1 (Kelly and Hawken 2017) indicated that 16% of V1 neurons were SMI-32-ir. Across all layers, 47% (268/571) of Kv3.1b-ir neurons were SMI-32-ir, exceeding the 16% rate in the overall population ($\chi 2(1) = 335$, $P < 0.001$). However, there was no difference in rate of SMI-32 immunoreactivity between Kv3.1b-ir, PV-ir and Kv3.1b-ir, non-PV-ir neurons (46% vs. 47% SMI-32-ir: $\chi 2(1) = 0.001$, $P > 0.05$, n.s.).

In the layers in which Kv3.1b-ir, non-PV-ir neurons were most abundant, approximately half of Kv3.1b-ir neurons were also SMI-32-ir. Of the Kv3.1b-ir, non-PV-ir neurons identified in layer 4B, 78% (14/19) were SMI-32-ir, and of the Kv3.1b-ir, non-PV-ir neurons from layer 4 Cα, 38% (17/45) were SMI-32-ir. The rate of SMI-32 expression was higher in Kv3.1b-ir, non-PV-ir neurons in layer 4B compared to layer 4 Cα ($\chi 2$ (1) = 9.44, $P < 0.005$), although not all Kv3.1b-ir, non-PV-ir neurons in layer 4B were SMI-32-ir. In layers 5 and 6, which included fewer Kv3.1b-ir, non-PV-ir neurons, all were SMI-32-ir.

Coexpression of PV and SMI-32

SMI-32-ir neurons were often PV-ir, which was unexpected because SMI-32 has been reported to primarily label pyramidal neurons (Campbell and Morrison 1989; Campbell et al. 1991; Vickers and Costa 1992; Hof and Morrison 1995; Hof et al. 1996), while PV labels non-pyramidal neurons (Hendry et al. 1989; Blümcke et al. 1990; Lewis and Lund 1990; Van Brederode et al. 1990). Recently, PV and SMI-32 were used to differentiate inhibitory and excitatory neurons, respectively, expressing Kv3.1b in primate motor cortex (Soares et al. 2017); however, our results suggest limited utility for SMI-32 as an excitatory cell marker, at least in V1. Coimmunoreactivity for PV and SMI-32 has been observed previously in macaque prefrontal cortex, but at a rate much lower than that observed in the present study (Vickers et al. 1993). SMI-32-ir, PV-ir neurons constituted a substantial proportion of both the total population of SMI-32-ir neurons (19%, 212 of 1126) and the total population of PV-ir neurons (43%, 212 of 480). All observed SMI-32-, PV-ir neurons were Kv3.1b-ir.

Because nearly all PV-ir neurons in V1 are GABAergic, coimmunoreactivity with PV suggested that SMI-32 labeled some GABAergic neurons. This was verified by examining 2 series of image stacks from tissue labeled with SMI-32, anti-PV, and anti-GABA (Fig. 8). SMI-32 and PV again labeled overlapping populations of neurons, and all identified SMI-32-ir, PV-ir neurons were GABA-ir. Therefore, SMI-32 immunoreactivity alone cannot reliably indicate that a neuron is excitatory. All observed examples of SMI-32-ir, GABA-ir neurons were PV-ir.

Morphology of Kv3.1b-ir Excitatory Neurons

Both the Meynert cells in layers 5 and 6 and the Meynert-Cajal cells in layer 4B have previously been observed to be Kv3.1b-ir (Ichinohe et al. 2004; Constantinople et al. 2009) and strongly SMI-32-ir (Hof and Morrison 1995; Chaudhuri et al. 1996; Hof et al. 1996, 2000). Examples of each cell type were observed in both sets of image series and were Kv3.1b-ir and non-PV-ir. It has previously been reported that most Betz cells in motor cortex (Preuss and Kaas 1996; Ichinohe et al. 2004) and 10% of Meynert cells (Ichinohe et al. 2004) were PV-ir. In the current study, we observed a few instances of Meynert cells that showed faint, diffuse fluorescence in the PV channel, but it did not resemble the weak PV immunoreactivity shown previously (Preuss and Kaas 1996; Ichinohe et al. 2004), nor was it similar to other weakly PV-ir somata we encountered. Instead, it appeared
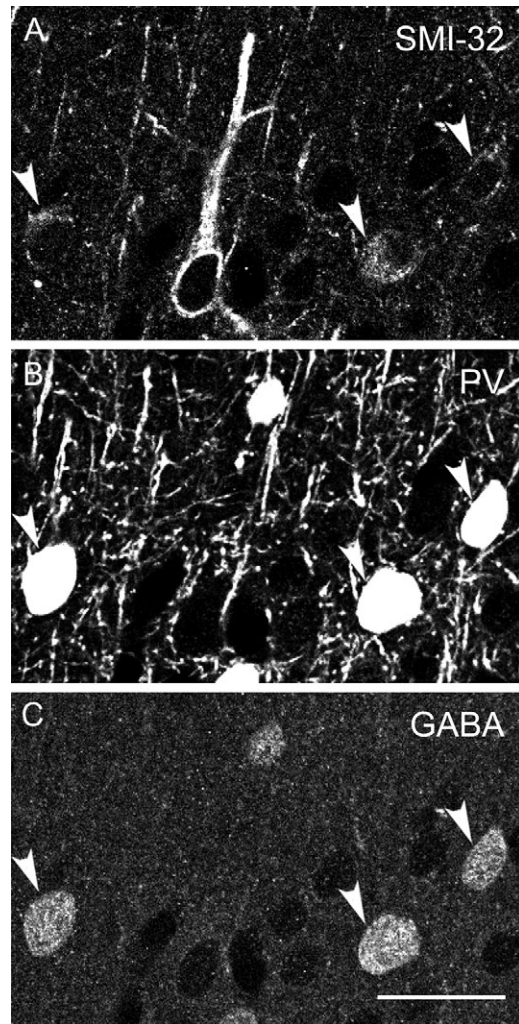

Figure 8. PV-, GABA-ir, and SMI-32-ir neurons. Confocal micrographs of tissue from animal M3 triple immunofluorescence labeled with SMI-32 (A), anti-PV (B), and anti-GABA (C). Arrowheads indicate examples of SMI-32-ir, PV-ir, GABA-ir neurons. Scale bar in C (refers to all panels): 25 μm.

to be out-of-focus light from the dense PV-ir basket terminals that consistently surrounded these neurons, and these cells were classified as non-PV-ir. Given that only 10% of Meynert cells were identified as PV-ir by Ichinohe et al (2004), it is possible that in our relatively small sampling of Meynert cells we happened not to encounter examples from this minority population, or that PV expression in these cells was so weak as to be lost below our low intensity threshold for this channel.

In layer 4 C, most excitatory neurons are spiny stellate cells (Valverde 1971; Lund 1973). We explored whether Kv3.1b-ir, non-GABA-ir, non-PV-ir neurons in layer 4 Cα had spiny stellate morphology by examining Kv3.1b and PV expression in BDA-filled neurons (Supplementary Methods). Following 2 1-mm-deep intracortical injections of BDA, labeled neurons were found across most cortical layers. Higher densities of filled neurons were found near the injection sites, but filled neurons were identified several mm from each injection site.

BDA filled both Kv3.1b-ir and non-Kv3.1b-ir neurons in layer 4 Cα. Some Kv3.1b-ir neurons were also PV-ir, likely indicating that BDA also filled inhibitory interneurons making local connections in V1. Several examples of BDA-labeled Kv3.1b-ir layer

4 Cα neurons lacked immunoreactivity for PV and had spiny stellate morphology (Supplementary Figs 5 and 6).

Discussion

The overall goal of the current study was to characterize the population of excitatory neurons in V1 that express the Kv3.1b potassium channel, which is critical for the fast-spiking properties associated with PV-expressing inhibitory interneurons (Du et al. 1996; Wang et al. 1998; Erisir et al. 1999; Hernández-Pineda et al. 1999; Rudy et al. 1999). We determined the distribution of Kv3.1b-ir, non-PV-ir, non-GABA-ir neurons across cortical depth and evaluated their SMI-32 coimmunoreactivity. In addition, we measured the density of GABAergic neurons in each cortical layer, including GABAergic neurons overall and the subset that coexpressed PV and/or Kv3.1b.

GABA-Immunoreactive Neurons

The densities of GABA-ir neurons in each cortical layer and across all layers of V1 (Fig. 3A; Supplementary Table 3) were very similar to previous stereologically measured densities of immunocytochemically identified neurons (Beaulieu et al. 1992). Our estimate of the average density across all layers of V1, 25 900 neurons/mm^3 was similar to the previously estimated 23 600 neurons/mm^3 (Beaulieu et al. 1992). However, because Beaulieu et al. (1992) reported much lower total neuronal densities than those from our more recent measurements (García-Marín et al. 2017; Kelly and Hawken 2017), the ratio of GABAergic neurons relative to the total population in the current study (11% in layers 2–6; Fig. 4B; Supplementary Table 3) was about half the previous estimate (Beaulieu et al. 1992).

Based on previously accepted results (Fitzpatrick et al. 1987; Hendry et al. 1987; Beaulieu et al. 1992), the excitatory-to-inhibitory neuron ratio in V1 has been considered to be between 3.8 and 5.7. Based on the results of the current study, this ratio is instead 8.1 (Fig. 4C). Accurately representing this ratio will be important for building functional models of primate cortex (Chariker et al. 2016) with realistic convergence of input to excitatory and inhibitory neuronal subpopulations.

Coexpression of PV, GABA, and Kv3.1b

The PV-ir population in macaque V1 was almost exclusively GABAergic and Kv3.1b-ir, and PV expression effectively captured the Kv3.1b-ir GABAergic subpopulation. As previously described, only a subset of GABA-ir neurons were PV-ir. In mouse somatosensory cortex, nearly the entire GABAergic population can be accounted for by 3 non-overlapping subpopulations expressing PV, somatostatin, or the ionotropic serotonin receptor 5-HT$_{3A}$ (Rudy et al. 2011). Particularly in light of known differences in developmental origin and diversity of interneurons between primates and rodents (Jones 2009; Rakic 2009; Zaitsev et al. 2009), it is uncertain whether the same 3 markers similarly capture the entire GABAergic population in primates. However, the calcium binding proteins PV, CB, and CR label largely non-overlapping subpopulations of GABAergic neurons in macaque cortex (Hendry et al. 1989; Vickers et al. 1993; Condé et al. 1994; Meskenaite 1997).

We found that 52% of GABA-ir neurons across all layers of macaque V1 and 79% of GABA-ir neurons in layer 4 C were PV-ir. Previously, Van Brederode et al (1990) reported that 74% of all GABA-ir neurons in V1 and nearly 100% of GABA-ir neurons in layer 4 C were PV-ir. Studies of calcium binding protein immunoreactivity in V1 (Kondo et al. 1994; Carder et al. 1996; Meskenaite 1997; Disney and Aoki 2008) and our own unpublished observations have identified small populations of CB- and CR-ir neurons in layer 4 C, which are likely GABAergic neurons that would be expected not to coexpress PV. In the current study, we used stereological exclusion boundaries to avoid counting biases that could have influenced the results of Van Brederode et al. (Van Brederode et al. 1990). In addition, we measured a lower ratio of GABA-ir to total neuronal density, similar numerical densities of GABA-ir neurons, and higher PV-ir densities relative to previous measurements (Fitzpatrick et al. 1987; Van Brederode et al. 1990; Beaulieu et al. 1992; Glezer et al. 1993; Carder et al. 1996; Sherwood et al. 2007), making it improbable that we underestimated the PV-ir population and/or overestimated the GABA-ir population. The overall pattern of PV coexpression in GABAergic neurons is similar to that observed in mice: 40% overall, and enriched in layer 4 (Tremblay et al. 2016).

The rates of coimmunoreactivity for Kv3.1b and PV across all layers measured in the present study (80% of Kv3.1b-ir neurons were PV-ir; 94% of PV-ir neurons were Kv3.1b-ir) were similar to the rates reported previously using confocal microscopy (Constantinople et al. 2009) (78% and 89%). Similarly, the proportion of Kv3.1b-ir neurons that were GABA-ir in this study (77%) was similar to that measured by Constantinople et al (2009) (71–76%) using confocal microscopy. In contrast, the proportion of GABA-ir neurons that were Kv3.1b-ir in this study (50%; 462 of 939 GABA-ir neurons) was substantially less than Constantinople et al (2009) measured using epifluorescence microscopy (85%; 1 121 of 1 313 GABA-ir neurons) and was closer to the proportion of GABAergic neurons coexpressing Kv3.1b and PV in mouse neocortex (Chow et al. 1999; Tremblay et al. 2016). This difference may be attributable to the different imaging methods used; confocal microscopy provided the resolution necessary for differentiating membrane expression of Kv3.1b from presynaptic staining of basket terminals.

Distribution and Functional Significance of Excitatory Kv3.1b-Immunoreactive Neurons

Excitatory pyramidal neurons—including presumptive Betz cells—exhibiting narrow spike widths have been identified in macaque primary motor and ventral premotor cortex (Vigneswaran et al. 2011). Betz cells, as well as other pyramidal neurons in primate motor cortex, express Kv3.1b (Ichinohe et al. 2004; Soares et al. 2017). In layers 4B and 4 Cα, 45% of Kv3.1b-ir neurons were non-GABA-ir, whereas in layer 2/3, 9% of Kv3.1b-ir neurons were non-GABA-ir. Therefore, if Kv3.1b immunoreactivity is a reliable correlate of narrow spiking, then our results suggest that approximately 45% of narrowly spiking neurons in layers 4B and 4 Cα and 9% in layer 2/3 are excitatory. These results suggest caution in using spike width to differentiate putatively inhibitory and excitatory neurons in monkey visual cortex (Mitchell et al. 2007; Chen et al. 2008; Anderson et al. 2011).

It is of great interest, therefore, to obtain physiological measurements from V1 neurons that are Kv3.1b-ir and not GABA-ir. It is possible that at least some Kv3.1b-ir, non-PV-ir neurons might resemble the chattering cells identified in layers 2, 3, and 4 of cat primary visual cortex, which included pyramidal neurons in layer 2/3 and a spiny stellate neuron in layer 4 (Nowak et al. 2003). In loose-patch juxtacellular recording experiments in our lab (Joshi and Hawken 2006), a subset of V1 neurons identified by morphology as excitatory have been observed to
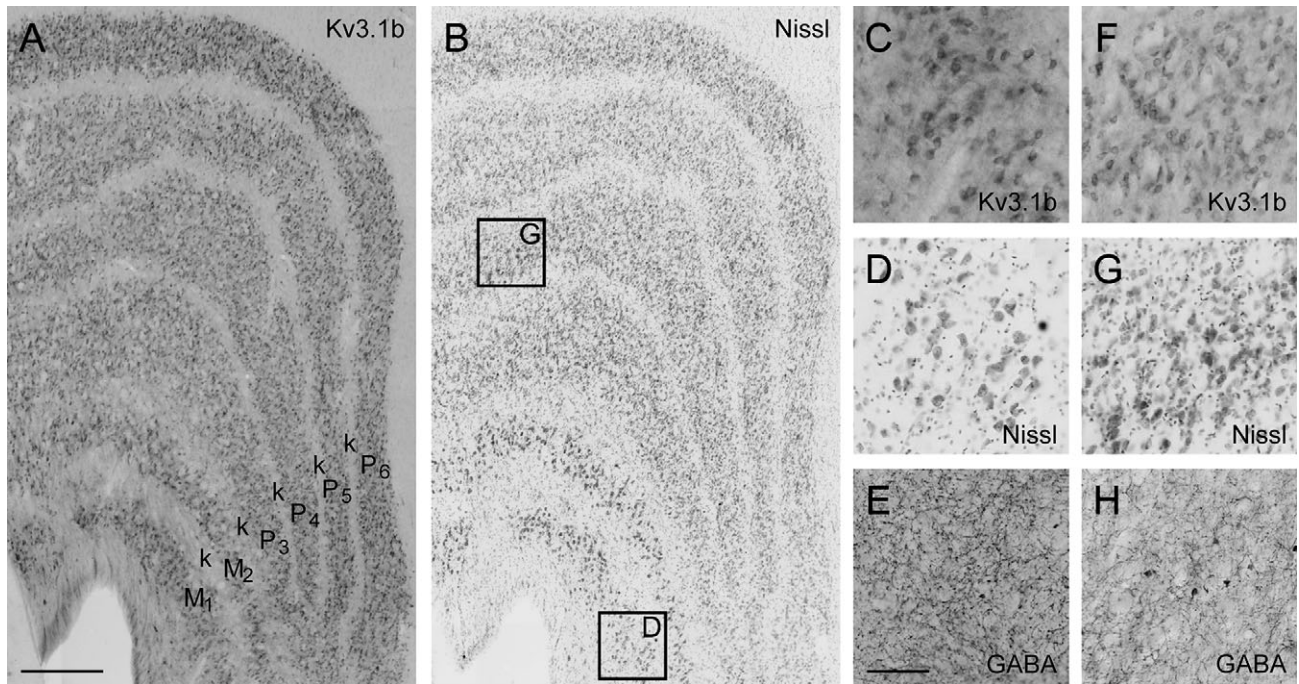
Figure 9. Kv3.1b in the LGN. (A): Micrograph of coronal section from dorsal LGN of monkey M5 showing pattern of Kv3.1b expression. (B): Adjacent Nissl stained section. (C–E): Enlarged view of Kv3.1b (C), Nissl (D), and GABA (E) staining in magnocellular layer 1 shows Kv3.1b-ir neurons are prevalent and may include the entire excitatory population. Location of enlarged region identified in (B). (F–H): Enlarged view of Kv3.1b (F), Nissl (G), and GABA (H) staining in parvocellular layer 4. Location of enlarged region identified in (B). Scale bar in (A) (refers to A and B): 500 μm. Scale bar in H (refers to C and H): 100 μm.

have strikingly narrow spike widths (Joshi 2007), but none of these have been evaluated for Kv3.1b expression.

Many Kv3.1b-ir, non-PV-ir, non-GABA-ir neurons were found within layers 4B and 4Cα, both of which are in the canonical M pathway. Specifically, 4% of all neurons in layer 4B and 8% of neurons in layer 4Cα were Kv3.1b-ir and neither PV-ir nor GABA-ir. In the lateral geniculate nucleus (LGN), Kv3.1b was expressed in many neurons in both M and P layers (Fig. 9), so the pattern of Kv3.1b expression in cortex may reflect laminar specificity rather than M pathway specificity. Nevertheless, Kv3.1b-ir excitatory neurons in V1 should disproportionately influence M pathway, rather than P pathway, processing.

The distribution of Kv3.1b-expressing excitatory neurons in V1 suggests that they are largely specific to the fastest feedforward cortical pathway to/through area MT. With the possible exception of a minor disynaptic geniculate input to MT (Nassi et al. 2006), signals propagating via layers 4Cα and 4B and via the Meynert and Cajal-Meynert cells in V1 are likely to be among the earliest inputs reaching MT. If Kv3.1b expression in this subset of excitatory neurons confers a fast spiking or stuttering phenotype, this could increase the fidelity of signal transmission from individual neurons in this direct feedforward cortical pathway and allow signals carried by small groups of neurons to propagate through cortical areas.

The tissue used for this study was sampled from opercular V1, allowing a comparison with previous estimates of total neuronal density from the same region (García-Marín et al. 2017; Kelly and Hawken 2017). The representation of the peripheral visual field, in the calcarine sulcus, was not sampled, and so it is possible our results will not generalize to this region. Neuronal density has been found to vary across V1 (Collins et al. 2010), though our neuronal density measurements (Kelly and Hawken 2017) were well matched to previous

results that included calcarine V1 (Giannaris and Rosene 2012). Densities of Meynert and Meynert-Cajal cells have been shown to increase with eccentricity (Hof and Morrison 1995). These were a minority of the Kv3.1b-ir, non-PV-ir, non-GABA-ir population we identified, and it is unknown whether the rest of this population might vary with eccentricity.

Species Specificity

To date, Kv3.1b expression has been observed to be highly specific to inhibitory neurons in rodent cortex; therefore, the presence of Kv3.1b-ir excitatory neurons in macaque cortex is an important difference between primate and rodent species. Humans and other primates have evolved an elaboration of the subventricular zone of the dorsal telencephalon and greater diversity of precursor cells, which may be critical in generating primate-specific types of cortical inhibitory interneurons (Petanjek et al. 2009; Rakic 2009; Zaitsev et al. 2009; Geschwind and Rakic 2013; Radonjić et al. 2014; Dehay et al. 2015). There is also considerable homology between Old World monkeys and great apes, including humans, in the early visual pathways (Solnitzky and Harman 1946; Kupfer et al. 1967; Stone and Johnston 1981; Kaas 2012), including the anatomical (Chacko 1948; Moskowitz and Noback 1962) and functional (Schneider et al. 2004; Denison et al. 2014; Zhang et al. 2015) M/P parcellation of the LGN. Therefore, human V1 may also have Kv3.1b-expressing excitatory neurons concentrated in layers 4Cα and 4B, as we have observed in macaque V1.

Supplementary Material

Supplementary material is available at *Cerebral Cortex* online.

Funding

Notes

References

Anderson EB, Mitchell JF, Reynolds JH. 2011. Attentional modulation of firing rate varies with burstiness across putative pyramidal neurons in macaque visual area V4. J Neurosci. 31:10983–10992.

Beaulieu C, Kisvarday Z, Somogyi P, Cynader M, Cowey A. 1992. Quantitative distribution of GABA-immunopositive and –immunonegative neurons and synapses in the monkey striate cortex (area 17). Cereb Cortex. 2:295–309.

Blümcke I, Hof PR, Morrison JH, Celio MR. 1990. Distribution of parvalbumin immunoreactivity in the visual cortex of old world monkeys and humans. J Comp Neurol. 301:417–432.

Brodmann K. 1909. Chapter I: The basic laminar pattern of the cerebral cortex. In: Garey LJ, editor. Localisation in the cerebral cortex. London (UK): Smith-Gordon. p. 13–36.

Campbell MJ, Hof PR, Morrison JH. 1991. A subpopulation of primate corticocortical neurons is distinguished by somato-dendritic distribution of neurofilament protein. Brain Res. 539:133–136.

Campbell MJ, Morrison JH. 1989. Monoclonal antibody to neurofilament protein (SMI-32) labels a subpopulation of pyramidal neurons in the human and monkey neocortex. J Comp Neurol. 282:191–205.

Carder RK, Leclerc SS, Hendry SHC. 1996. Regulation of calcium-binding protein immunoreactivity in GABA neurons of macaque primary visual cortex. Cereb Cortex. 6:271–287.

Cauli B, Audinat E, Lambolez B, Angulo MC, Ropert N, Tsuzuki K, Hestrin S, Rossier J. 1997. Molecular and physiological diversity of cortical nonpyramidal cells. J Neurosci. 17: 3894–3906.

Cavanaugh JR, Bair W, Movshon JA. 2002. Nature and interaction of signals from the receptive field center and surround in macaque V1 neurons. J Neurophysiol. 88:2530–2546.

Celio MR. 1986. Parvalbumin in most γ-aminobutyric acid-containing neurons of the rat cerebral cortex. Science. 231: 995–997.

Chacko LW. 1948. The laminar pattern of the lateral geniculate body in the primates. J Neurol Neurosurg Psychiatry. 11: 211–224.

Chariker L, Shapley R, Young L-S. 2016. Orientation selectivity from very sparse LGN inputs in a comprehensive model of macaque V1 cortex. J Neurosci. 26:12368–12384.

Chaudhuri A, Zangenehpour S, Matsubara JA, Cynader MS. 1996. Differential expression of neurofilament protein in the visual system of the vervet monkey. Brain Res. 709:17–26.

Chen Y, Martinez-Conde S, Macknik SL, Bereshpolova Y, Swadlow HA, Alonso J-M. 2008. Task difficulty modulates the activity of specific neuronal populations in primary visual cortex. Nat Neurosci. 11:974–982.

Chow A, Erisir A, Nadal MS, Ozaita A, Lau D, Welker E, Rudy B. 1999. K+ channel expression distinguishes subpopulations of parvalbumin- and somatostatin-containing neocortical interneurons. J Neurosci. 19:9332–9345.

Collins CE, Airey DC, Young NA, Leitch DB, Kaas JH. 2010. Neuron densities vary across and within cortical areas in primates. Proc Natl Acad Sci USA. 107:15927–15932.

Condé F, Lund JS, Jacobowitz DM, Baimbridge KG, Lewis DA. 1994. Local circuit neurons immunoreactive for calretinin, calbindin D-28k or parvalbumin in monkey prefrontal cortex: Distribution and morphology. J Comp Neurol. 341: 95–116.

Constantinople CM, Disney AA, Maffie J, Rudy B, Hawken MJ. 2009. Quantitative analysis of neurons with Kv3 potassium channel subunits, Kv3.1b and Kv3.2, in macaque primary visual cortex. J Comp Neurol. 516:291–311.

DeFelipe J, Alonso-Nanclares L, Blatow M, Caputi A, Monyer H. 2006. Anatomical and molecular heterogeneity of cortical GABAergic interneurons. In: Grillner S, Graybiel A, editors. Microcircuits: the interface between neurons and global brain function. Dahlem Workshop Report 93. Cambridge (MA): The MIT Press. p. 295–325.

Dehay C, Kennedy H, Kosik KS. 2015. The outer subventricular zone and primate-specific cortical complexification. Neuron. 85:683–694.

Denison RN, Vu AT, Yacoub E, Feinberg DA, Silver MA. 2014. Functional mapping of the magnocellular and parvocellular subdivisions of human LGN. NeuroImage. 102: 358–369.

Disney AA, Aoki C. 2008. Muscarinic acetylcholine receptors in macaque V1 are most frequently expressed by parvalbumin-immunoreactive neurons. J Comp Neurol. 507:1748–1762.

Disney AA, Reynolds JH. 2014. Expression of m1-type muscarinic acetylcholine receptors by parvalbumin-immunoreactive neurons in the primary visual cortex: a comparative study of rat, guinea pig, ferret, macaque, and human. J Comp Neurol. 522:986–1003.

Du J, Zhang L, Weiser M, Rudy B, McBain CJ. 1996. Developmental expression and functional characterization of the potassium-channel subunit Kv3.1b in parvalbumin-containing interneurons of the rat hippocampus. J Neurosci. 16:506–518.

Erisir A, Lau D, Rudy B, Leonard CS. 1999. Function of specific K$^+$ channels in sustained high-frequency firing of fast-spiking neocortical interneurons. J Neurophysiol. 82:2476–2489.

Fenstemaker SB, Kiorpes L, Movshon JA. 2001. Effects of experimental strabismus on the architecture of macaque monkey striate cortex. J Comp Neurol. 438:300–317.

Fitzpatrick D, Lund JS, Schmechel DE, Towles AC. 1987. Distribution of GABAergic neurons and axon terminals in the macaque striate cortex. J Comp Neurol. 264:73–91.

Fries W, Distel H. 1983. Large layer VI neurons of monkey striate cortex (Meynert cells) project to the superior colliculus. Proc R Soc Lond B. 219:53–59.

Fries W, Keizer K, Kuypers HG. 1985. Large layer VI cells in macaque striate cortex (Meynert cells) project to both superior colliculus and prestriate visual area V5. Exp Brain Res. 58:613–616.

García-Marín V, Ahmed TH, Afzal YC, Hawken MJ. 2013. Distribution of the vesicular glutamate transporter 2

(vGluT2) in the primary visual cortex of the macaque and human. J Comp Neurol. 521:130–151.

García-Marín V, Kelly JG, Hawken MJ. 2017. Major feedforward thalamic input into layer 4C of primary visual cortex in primate. Cereb Cortex. doi:10.1093/cercor/bhx311.

Geschwind DH, Rakic P. 2013. Cortical evolution: judge the brain by its cover. Neuron. 80:633–647.

Giannaris EL, Rosene DL. 2012. A stereological study of the numbers of neurons and glia in the primary visual cortex across the lifespan of male and female rhesus monkeys. J Comp Neurol. 520:3492–3508.

Glezer II, Hof PR, Leranth C, Morgane PJ. 1993. Calcium-binding protein-containing neuronal populations in mammalian visual cortex: a comparative study in whales, insectivores, bats, rodents, and primates. Cereb Cortex. 3: 249–272.

Goris RLT, Simoncelli EP, Movshon JA. 2015. Origin and function of tuning diversity in macaque visual cortex. Neuron. 88: 819–831.

Gundersen HJ, Bendtsen TF, Korbo L, Marcussen N, Møller A, Nielsen K, Nyengaard JR, Pakkenberg B, Sørensen FB, Vesterby A, et al. 1988. Some new, simple and efficient stereological methods and their use in pathological research and diagnosis. APMIS. 96:379–394.

Hendry SHC, Jones EG, Emson PC, Lawson DEM, Heizmann CW, Streit P. 1989. Two classes of cortical GABA neurons defined by differential calcium binding protein immunoreactivities. Exp Brain Res. 76:467–472.

Hendry SH, Schwark HD, Jones EG, Yan J. 1987. Numbers and proportions of GABA-immunoreactive neurons in different areas of monkey cerebral cortex. J Neurosci. 7:1503–1519.

Hernández-Pineda R, Chow A, Amarillo Y, Moreno H, Saganich M, Vega-Saenz de Miera E, Hernández-Cruz A, Rudy B. 1999. Kv3.1-Kv3.2 channels underlie a high-voltage – activating component of the delayed rectifier K^+ current in projecting neurons from the globus pallidus. J Neurophysiol. 82: 1512–1528.

Hof PR, Morrison JH. 1995. Neurofilament protein defines regional patterns of cortical organization in the macaque monkey visual system: A quantitative immunohistochemical analysis. J Comp Neurol. 352:161–186.

Hof PR, Nimchinsky EA, Young WG, Morrison JH. 2000. Numbers of Meynert and layer IVB cells in area V1: a stereologic analysis in young and aged macaque monkeys. J Comp Neurol. 420:113–126.

Hof PR, Ungerleider LG, Webster MJ, Gattass R, Adams MM, Sailstad CA, Morrison JH. 1996. Neurofilament protein is differentially distributed in subpopulations of corticocortical projection neurons in the macaque monkey visual pathways. J Comp Neurol. 376:112–127.

Horton JC. 1984. Cytochrome oxidase patches: a new cytoarchitectonic feature of monkey visual cortex. Philos Trans R Soc Lond B. 304:199–253.

Horton JC, Hedley-Whyte ET. 1984. Mapping of cytochrome oxidase patches and ocular dominance columns in human visual cortex. Philos Trans R Soc Lond B. 304:255–272.

Howard V, Reid S, Baddeley A, Boyde A. 1985. Unbiased estimation of particle density in the tandem scanning reflected light microscope. J Microsc. 138:203–212.

Härtig W, Derouiche A, Welt K, Brauer K, Grosche J, Mäder M, Reichenbach A, Brückner G. 1999. Cortical neurons immunoreactive for the potassium channel Kv3.1b subunit are predominantly surrounded by perineuronal nets presumed as a buffering system for cations. Brain Res. 842:15–29.

Ichinohe N, Watakabe A, Miyashita T, Yamamori T, Hashikawa T, Rockland KS. 2004. A voltage-gated potassium channel, Kv3.1b, is expressed by a subpopulation of large pyramidal neurons in layer 5 of the macaque monkey cortex. Neurosci. 129:179–185.

Jones EG. 2009. The origins of cortical interneurons: mouse versus monkey and human. Cereb Cortex. 19:1953–1956.

Joshi S. 2007. Structure-function relations in macaque V1 [dissertation]. New York (NY): New York University. Retrieved from: ProQuest Dissertations & Theses Global. (3269787).

Joshi S, Hawken MJ. 2006. Loose-patch-juxtacellular recording in vivo—a method for functional characterization and labeling of neurons in macaque V1. J Neurosci Methods. 156:37–49.

Kaas JH. 2012. The evolution of neocortex in primates. Prog Brain Res. 195:91–102.

Kawaguchi Y, Kubota Y. 1993. Correlation of physiological subgroupings of nonpyramidal cells with parvalbumin- and calbindin$_{D28k}$-immunoreactive neurons in layer V of rat frontal cortex. J Neurophysiol. 70:387–396.

Kawaguchi Y, Kubota Y. 1998. Neurochemical features and synaptic connections of large physiologically-identified GABAergic cells in the rat frontal cortex. Neurosci. 85:677–701.

Kelly JG, Hawken MJ. 2017. Quantification of neuronal density across cortical depth using automated 3D analysis of confocal image stacks. Brain Struct Funct. 222:3333–3353.

Kondo H, Hashikawa T, Tanaka K, Jones EG. 1994. Neurochemical gradient along the monkey occipito-temporal cortical pathway. NeuroReport. 5:613–616.

Kupfer C, Chumbley L, Downer JC. 1967. Quantitative histology of optic nerve, optic tract and lateral geniculate nucleus of man. J Anat. 101:393–401.

Labro AJ, Priest MF, Lacroix JJ, Snyders DJ, Bezanilla F. 2015. K_v3.1 uses a timely resurgent K+ current to secure action potential repolarization. Nat Commun. 6:10173.

Lewis DA, Lund JS. 1990. Heterogeneity of chandelier neurons in monkey neocortex: Corticotropin-releasing factor- and parvalbumin-immunoreactive populations. J Comp Neurol. 293:599–615.

Lund JS. 1973. Organization of neurons in the visual cortex, area 17, of the monkey (*Macaca mulatta*). J Comp Neurol. 147: 455–496.

Lund JS, Lund RD, Hendrickson AE, Bunt AH, Fuchs AF. 1975. The origin of efferent pathways from the primary visual cortex, area 17, of the macaque monkey as shown by retrograde transport of horseradish peroxidase. J Comp Neurol. 164:287–304.

Meskenaite V. 1997. Calretinin-immunoreactive local circuit neurons in area 17 of the cynomolgus monkey, *Macaca fascicularis*. J Comp Neurol. 379:113–132.

Mitchell JF, Sundberg KA, Reynolds JH. 2007. Differential attention-dependent response modulation across cell classes in macaque visual area V4. Neuron. 55:131–141.

Morrison JH, Hof PR, Huntley GW. 1998. Neurochemical organization of the primate visual cortex. In: Bloom FE, Björklund A, Hökfelt T, editors. Handbook of chemical neuroanatomy, Vol. 14. The Primate Nervous System, Part H. New York (NY): Elsevier Science. p. 299–430.

Moskowitz N, Noback CR. 1962. The human lateral geniculate body in normal development and congenital unilateral anophthalmia. J Neuropathol Exp Neurol. 21:377–382.

Nassi JJ, Lyon DC, Callaway EM. 2006. The parvocellular LGN provides a robust disynaptic input to the visual motion area MT. Neuron. 50:319–237.

Nhan HL, Callaway EM. 2012. Morphology of superior-colliculus- and middle temporal area-projecting neurons in primate primary visual cortex. J Comp Neurol. 520:52–80.

Nowak LG, Azouz R, Sanchez-Vives MV, Gray CM, McCormick DA. 2003. Electrophysiological classes of cat primary visual cortical neurons in vivo as revealed by quantitative analyses. J Neurophysiol. 89:1541–1566.

O'Kusky J, Colonnier M. 1982. A laminar analysis of the number of neurons, glia, and synapses in the adult cortex (area 17) of adult macaque monkeys. J Comp Neurol. 210:278–290.

Petanjek Z, Berger B, Esclapez M. 2009. Origins of cortical GABAergic neurons in the cynomolgous monkey. Cereb Cortex. 19:249–262.

Povysheva NV, Zaitsev AV, Rotaru DC, Gonzalez-Burgos G, Lewis DA, Krimer LS. 2008. Parvalbumin-positive basket interneurons in monkey and rat prefrontal cortex. J Neurophysiol. 100:2348–2360.

Preuss TM, Kaas JH. 1996. Parvalbumin-like immunoreactivity of layer V pyramidal cells in the motor and somatosensory cortex of adult primates. Brain Res. 712:353–357.

Radonjić NV, Ayoub AE, Memi F, Yu X, Maroof A, Jakovcevski I, Anderson SA, Rakic P, Zecevic N. 2014. Diversity of cortical interneurons in primates: The role of the dorsal proliferative niche. Cell Rep. 9:2139–2151.

Rakic P. 2009. Evolution of the neocortex: a perspective from developmental biology. Nat Rev Neurosci. 10:724–735.

Renier N, Wu Z, Simon DJ, Yang J, Ariel P, Tessier-Lavigne M. 2014. iDISCO: a simple, rapid method to immunolabel large tissue samples for volume imaging. Cell. 159:896–910.

Rudy B, Chow A, Lau D, Amarillo Y, Ozaita A, Saganich M, Moreno H, Nadal MS, Hernández-Pineda R, Hernández-Cruz A, et al. 1999. Contributions of Kv3 channels to neuronal excitability. Ann N Y Acad Sci. 868:304–343.

Rudy B, Fishell G, Lee S, Hjerling-Leffler J. 2011. Three groups of interneurons account for nearly 100% of neocortical GABAergic neurons. Dev Neurobiol. 71:45–61.

Rudy B, McBain CJ. 2001. Kv3 channels: voltage-gated K$^+$ channels designed for high-frequency repetitive firing. Trends Neurosci. 24:517–526.

Schneider CA, Rasband WS, Eliceiri KW. 2012. NIH Image to ImageJ: 25 years of image analysis. Nat Methods. 9:671–675.

Schneider KA, Richter MC, Kastner S. 2004. Retinotopic organization and functional subdivisions of the human lateral geniculate nucleus: a high-resolution functional magnetic resonance imaging study. J Neurosci. 24:8975–8985.

Seligman AM, Karnovsky MJ, Wasserkrug HL, Hanker JS. 1968. Nondroplet ultrastructural demonstration of cytochrome oxidase activity with a polymerizing osmiophilic reagent, diaminobenzidine (DAB). J Cell Biol. 38:1–14.

Sherwood CC, Raghanti MA, Stimpson CD, Bonar CJ, deSousa AA, Preuss TM, Hof PR. 2007. Scaling of inhibitory interneurons in areas V1 and V2 of anthropoid primates as revealed by calcium binding protein immunohistochemistry. Brain Behav Evol. 69:176–195.

Shi SR, Key ME, Kalra KL. 1991. Antigen retrieval in formalin-fixed, paraffin-embedded tissues: An enhancement method for immunohistochemical staining based on microwave oven heating of tissue sections. J Histochem Cytochem. 39: 741–748.

Sincich LC, Horton JC. 2005. The circuitry of V1 and V2: integration of color, form, and motion. Annu Rev Neurosci. 28: 303–326.

Soares JGM, de Castro PHR, Fiorani M, Nascimento-Silva S, Gattass R. 2008. Distribution of neurofilament proteins in the lateral geniculate nucleus, primary visual cortex, and area MT of adult Cebus monkeys. J Comp Neurol. 508:605–614.

Soares D, Goldrick I, Lemon RN, Kraskov A, Greensmith L, Kalmar B. 2017. Expression of Kv3.1b potassium channel is widespread in macaque motor cortex pyramidal cells: A histological comparison between rat and macaque. J Comp Neurol. 525:2164–2174.

Solnitzky O, Harman PJ. 1946. A comparative study of the central and peripheral sectors of the visual cortex in primates, with observations on the lateral geniculate body. J Comp Neurol. 85:313–419.

Solomon SG, Peirce JW, Lennie P. 2004. The impact of suppressive surrounds on chromatic properties of cortical neurons. J Neurosci. 24:148–160.

Sterio DC. 1984. The unbiased estimation of number and sizes of arbitrary particles using the disector. J Microsc. 134: 127–136.

Sternberger LA, Sternberger NH. 1983. Monoclonal antibodies distinguish phosphorylated and nonphosphorylated forms of neurofilaments in situ. Proc Natl Acad Sci USA. 80: 6126–6130.

Stone J, Johnston E. 1981. The topography of primate retina: a study of the human, bushbaby, and new- and old-world monkeys. J Comp Neurol. 196:205–223.

Tremblay R, Lee S, Rudy B. 2016. GABAergic interneurons in the neocortex: from cellular properties to circuits. Neuron. 91: 260–292.

Trujillo-Cenóz O, Fernández A, Radmilovich M, Reali C, Russo RE. 2007. Cytological organization of the central gelatinosa in the turtle spinal cord. J Comp Neurol. 502:291–308.

Valverde F. 1971. Short axon neuronal subsystems in the visual cortex of the monkey. Int J Neurosci. 1:181–197.

Van Brederode JFM, Mulligan KA, Hendrickson AE. 1990. Calcium-binding proteins as markers for subpopulations of GABAergic neurons in monkey striate cortex. J Comp Neurol. 298:1–22.

Vickers JC, Costa M. 1992. The neurofilament triplet is present in distinct subpopulations of neurons in the central nervous system of the guinea-pig. Neurosci. 49:73–100.

Vickers JC, Huntley GW, Edwards AM, Moran T, Rogers SW, Heinemann SF, Morrison JH. 1993. Quantitative localization of AMPA/kainate and kainate glutamate receptor subunit immunoreactivity in neurochemically identified subpopulations of neurons in the prefrontal cortex of the macaque monkey. J Neurosci. 13:2962–2992.

Vigneswaran G, Kraskov A, Lemon RN. 2011. Large identified pyramidal cells in macaque motor and premotor cortex exhibit "thin spikes": implications for cell type classification. J Neurosci. 31:14235–14242.

Wang L-Y, Gan L, Forsythe ID, Kaczmarek LK. 1998. Contribution of the Kv3.1 potassium channel to high-frequency firing in mouse auditory neurones. J Physiol. 509:183–194.

Weiser M, Bueno E, Sekirnjak C, Martone ME, Baker H, Hillman D, Chen S, Thornhill W, Ellisman M, Rudy B. 1995. The potassium channel subunit Kv3.1b is localized to somatic and axonal membranes of specific populations of CNS neurons. J Neurosci. 15:4298–4314.

Weiser M, Vega-Saenz de Miera E, Kentros C, Moreno H, Franzen L, Hillman D, Baker H, Rudy B. 1994. Differential expression of Shaw-related K$^+$ channels in the rat central nervous system. J Neurosci. 14:949–972.

Williams RW, Rakic P. 1988. Three-dimensional counting: an accurate and direct method to estimate numbers of cells in sectioned material. J Comp Neurol. 278:344–352.

Wong-Riley M. 1979. Changes in the visual system of monocularly sutured or enucleated cats demonstrable with cytochrome oxidase histochemistry. Brain Res. 171:11–28.

Xing D, Ringach DL, Shapley R, Hawken MJ. 2004. Correlation of local and global orientation and spatial frequency tuning in macaque V1. J Physiol. 557:923–933.

Zaitsev AV, Gonzalez-Burgos G, Povysheva NV, Kröner S, Lewis DA, Krimer LS. 2005. Localization of calcium-binding proteins in physiologically and morphologically characterized interneurons of monkey dorsolateral prefrontal cortex. Cereb Cortex. 15:1178–1186.

Zaitsev AV, Povysheva NV, Gonzalez-Burgos G, Rotaru D, Fish K, Krimer LS, Lewis DA. 2009. Interneuron diversity in layers 2–3 of monkey prefrontal cortex. Cereb Cortex. 19:1597–1615.

Zhang P, Zhou H, Wen W, He S. 2015. Layer-specific response properties of the human lateral geniculate nucleus and superior colliculus. NeuroImage. 111:159–166.